

The copyright of this thesis vests in the author. No quotation from it or information derived from it is to be published without full acknowledgement of the source. The thesis is to be used for private study or non-commercial research purposes only.

Published by the University of Cape Town (UCT) in terms of the non-exclusive license granted to UCT by the author.

INVESTIGATION OF A COMPUTATIONALLY PREDICTED STRUCTURE IN THE Ag-Pt SYSTEM



Soraya Allies

**A dissertation submitted to the Faculty of Engineering and the
Built Environment in fulfilment of the requirements for the degree
of Master of Science in Engineering**

February 2013

DECLARATIONS

- i. I hereby grant the University of Cape Town free license to reproduce for the purpose of research either the whole or any portion of the contents in any manner whatsoever of this dissertation. I am presenting this dissertation in **full** fulfilment of the requirements for my degree.

- ii. I know the meaning of plagiarism and declare that all of the work in the document, save for that which is properly acknowledged, is my own.

Signed by candidate

Signature: Signature Removed

Date: 07 February 2013

University of Cape Town

ACKNOWLEDGEMENTS

I would like to thank God for making all of this possible. I would also like to express my sincere gratitude and appreciation to the following people:

- Professor Candace Lang for all her love, encouragement and guidance throughout this project
- Professor Robert Knutsen for being the *diligens paterfamilias* (good father of the family)
- Penny Park-Ross for being the Centre for Materials Engineering (CME) mother and her knowledge about everything!
- The Centre for High Resolution Transmission Electron Microscopy (HRTEM) at Nelson Mandela Metropolitan University (NMMU) especially Professor Michael Lee, Jacques O'Connell and a special thank you to Professor Jan Neethling for the computational modelling of the possible structure and all the hours put in to solving this structure
- The Electron Microscope Unit at the University of Cape Town (UCT) especially Miranda Waldron, Mohammed Jaffer and Franscious Cummings
- Chumani Mshumi for teaching me to use the Transmission Electron Microscope (TEM) and specimen preparation
- Dr Sarah George for teaching me to use the Differential Scanning Calorimeter (DSC) and her assistance in interpreting the results
- The National Research Foundation for funding myself and the project
- Dineo Ngwenya and Velile Vilane for all the fun times in 218
- All the students and staff at CME for all the cake and laughter
- Last but not least, Shaun von Willingh for getting me through this overwhelming period.

ABSTRACT

Computational modelling is fast becoming the chosen way to predict novel structures. These structures need to be validated in order to gain credibility and generate more confidence in computational predictions. This investigation of the equiatomic region of the Ag-Pt system shows that computational modelling can be used successfully as a precursor to experimental investigations.

Various techniques including electron microscopy, hardness and Differential Scanning Calorimetry were used to investigate different properties of the alloy. These techniques have shown that an ordered phase may exist in the Ag-Pt system. This ordered phase has been shown to have an increased hardness and has produced extra reflections in electron diffraction patterns. Scanning Electron Microscope equipped with a Backscattered Electron detector has shown that a third phase is present in the alloy and the composition is close to 50:50; within experimental error.

The alloys showed considerable inhomogeneity and it was not homogenised prior to or post cold rolling. This could be a reason for the third phase not reaching an equilibrium state after prolonged heat treatments. The final structure might be the $L1_1$ structure but the full transformation is slow and further investigation is required. It is recommended that future research be carried out taking into account the recommendations provided in Chapter 7.

TABLE OF CONTENTS

	Page
DECLARATIONS	I
ACKNOWLEDGEMENTS	II
ABSTRACT	III
TABLE OF CONTENTS	IV
LIST OF FIGURES	VII
LIST OF TABLES	X
LIST OF ABBREVIATIONS	X
1 INTRODUCTION.....	1
1.1 BACKGROUND	1
1.2 THE SILVER-PLATINUM ALLOY SYSTEM	1
1.3 OBJECTIVES	2
1.4 LIMITATIONS AND SCOPE OF THESIS	2
1.5 PLAN OF DEVELOPMENT	2
2 LITERATURE REVIEW	3
2.1 THE SILVER-PLATINUM SYSTEM: PREVIOUS EXPERIMENTAL WORK	3
2.2 COMPUTATIONAL PREDICTIONS OF ORDERING IN THE SILVER- PLATINUM SYSTEM	11
2.3 ORDERING	17
2.4 THE L ₁ ORDERED STRUCTURE	19
3 EXPERIMENTAL PROCEDURES.....	21
3.1 ALLOY PREPARATION	21

3.2	SPECIMEN PREPARATION	21
3.3	HEAT TREATMENTS	21
3.4	METALLOGRAPHY	21
3.4.1.	<i>GRINDING</i>	21
3.4.2.	<i>POLISHING</i>	22
3.5	HARDNESS	22
3.6	DIFFERENTIAL SCANNING CALORIMETRY (DSC)	22
3.7	SCANNING ELECTRON MICROSCOPY (SEM)	23
3.7.1	<i>ENERGY DISPERSIVE X-RAY SPECTROSCOPY (EDS)</i>	23
3.7.2	<i>FOCUSED ION BEAM (FIB)</i>	24
3.8	TRANSMISSION ELECTRON MICROSCOPY (TEM)	24
4	RESULTS	25
4.1	THE EFFECT OF HEAT TREATMENT ON MICROSTRUCTURE	25
4.1.1	<i>AS-CAST</i>	25
4.1.2	<i>20 DAYS AT 750°C</i>	26
4.1.3	<i>40 DAYS AT 750°C</i>	27
4.1.4	<i>60 DAYS AT 750°C</i>	28
4.1.5	<i>80 DAYS AT 750°C</i>	30
4.1.6	<i>40 DAYS AT 850°C</i>	31
4.2	THE EFFECT OF HEAT TREATMENT ON HARDNESS	32
4.3	DISSOLUTION TEMPERATURES USING DSC	33
4.4	CRYSTAL STRUCTURE ANALYSIS USING ELECTRON DIFFRACTION	35
5	DISCUSSION.....	40
5.1	EFFECT OF HEAT TREATMENT ON MICROSTRUCTURE	40
5.2	HARDNESS	40
5.3	DSC	41

5.4	TEM	41
5.5	OVERVIEW	42
6	CONCLUSIONS.....	43
7	RECOMMENDATIONS.....	44
8	REFERENCES.....	50

University of Cape Town

LIST OF FIGURES

Figure 2.1.1 Phase diagram for the Ag-Pt system, after Doerinckel ⁵	4
Figure 2.1.2 Phase diagram for the Ag-Pt system, after Kurnakow and Nemilow ⁶ ...	4
Figure 2.1.3 Graph showing electrical resistivity vs composition of Ag-Pt alloys at different temperatures, after Johansson and Linde ⁷	5
Figure 2.1.4 Phase diagram for the Ag-Pt system, after Johansson and Linde ⁷ (● – Electrical resistivity measurements, ○ – X-ray diffraction measurements).....	5
Figure 2.1.5 Phase diagram for the Ag-Pt system, after Schneider and Esch ⁹ (X - X-ray crystallographic measurements and ○ – conductivity measurements).....	6
Figure 2.1.6 Phase diagram for the Ag-Pt system, after Novikova and Rudnitskii ¹⁰ ..	7
Figure 2.1.7 Revised phase diagram for the Ag-Pt system, after Klement and Luo ⁹ .	8
Figure 2.1.8 Lattice parameters of FCC solid solutions in Ag-Pt alloys ¹¹	9
Figure 2.1.9 The most recent Ag-Pt phase diagram, after Durussel and Feschotte ³	10
Figure 2.2.1 Assessed phase diagram for the Ag-Pt system, by Karakaya and Thompson ¹⁵	12
Figure 2.2.2 a) Calculated heats of formation with relativistic correction and	13
Figure 2.2.3 Formation enthalpies of ordered structures in the Ag-Pt system ¹⁸	14
Figure 2.2.4 Computed phase diagram for the Ag-Pt system ¹⁸	14
Figure 2.2.5 Low temperature ground states for the Ag-Pt system ¹	15
Figure 2.3.1 (a) An example of a disordered copper-gold lattice and (b) The ordered structure of Cu ₃ Au (L1 ₂) ¹⁷	18
Figure 2.4.1 Distribution of atoms at the composition CuPt showing the alternate (111) planes that are occupied by Cu and Pt atoms ¹⁷	19
Figure 2.4.2 (a) Primitive unit cell for FCC-lattice with lattice parameter a (disordered state). (b) Ordered rhombohedral unit cell of CuPt with new lattice parameter 2a ²⁴	19
Figure 3.6.1 DTA of Ag _{50.08} Pt _{49.92} annealed at 600°C for 300 days ³	22

Figure 4.1.1 BSE micrograph and compositional analysis of Ag 54±1 at.% Pt as-cast.	25
Figure 4.1.2 BSE micrograph and compositional analysis of Ag 51±1 at.% Pt as-cast.	26
Figure 4.1.3 BSE micrograph and compositional analysis of Ag 54±1 at.% Pt after 20 days at 750°C.	26
Figure 4.1.4 BSE micrograph and compositional analysis of Ag 51±1 at.% Pt after 20 days at 750°C.	27
Figure 4.1.5 BSE micrograph and compositional analysis of Ag 54±1 at.% Pt after 40 days at 750°C.	27
Figure 4.1.6 BSE micrograph and compositional analysis of Ag 51±1 at.% Pt after 40 days at 750°C.	28
Figure 4.1.7 BSE micrograph and compositional analysis of Ag 54±1 at.% Pt after 60 days at 750°C.	28
Figure 4.1.8 BSE micrograph and compositional analysis of Ag 51±1 at.% Pt after 60 days at 750°C.	29
Figure 4.1.9 BSE micrograph and compositional analysis of Ag 54±1 at.% Pt after 80 days at 750°C.	30
Figure 4.1.10 BSE micrograph and compositional analysis of Ag 51±1 at.% Pt after 80 days at 750°C.	30
Figure 4.1.11 BSE micrograph and compositional analysis of Ag 54±1 at.% Pt after 40 days at 850°C.	31
Figure 4.1.12 BSE micrograph and compositional analysis of Ag 51±1 at.% Pt after 40 days at 850°C.	31
Figure 4.2.1 Vickers hardness of alloys showing an increase in hardness at 750°C and decrease in hardness at 850°C.	32
Figure 4.3.1 DSC results for Ag 54±1 at.% Pt.	33
Figure 4.3.2 DSC results for Ag 51±1 at.% Pt.	34
Figure 4.4.1 Electron diffraction pattern for cold rolled Ag 54±1 at.% Pt, viewed along the [100] _{fcc} zone axis.	35

Figure 4.4.2 Electron diffraction pattern for cold rolled Ag 51±1 at.% Pt, viewed along the $[100]_{\text{fcc}}$ zone axis.....	35
Figure 4.4.3 Electron diffraction pattern for Ag 51±1 at.% Pt, heat treated at 750°C for 80 days, possibly viewed along the $[100]_{\text{fcc}}$ zone axis.	36
Figure 4.4.4 Bright field (left) and dark field (right) pair obtained using additional reflection in Figure 4.4.3.	36
Figure 4.4.5 Electron diffraction pattern for Ag 54±1 at.% Pt, heat treated at 750°C for 60 days, possibly viewed along the $[100]_{\text{fcc}}$ zone axis.	37
Figure 4.4.6 Electron diffraction patterns for (a) Ag 54±1 at.% Pt after 60 days at 750°C, prepared by FIB SEM; (b) Ag 51±1 at.% Pt after 80 days at 750°C, prepared by PIPS.....	38
Figure 4.4.7 (a) Simulated electron diffraction pattern showing additional spots expected from $L1_1$ in $[112]$ zone axis diffraction pattern; (b) experimental diffraction pattern.....	38
Figure 4.4.8 Bright-field TEM image of (a) Ag 51±1 at.% Pt after 80 days at 750°C; and (b) Ag 54±1 at.% Pt after 60 days at 750°C, showing modulated microstructure.	39
Figure 5.4.1 TEM bright-field images and electron diffraction patterns, acquired from a U-6wt%Nb alloy after ageing (after Hsiung and Zhou ²⁶).	42
Figure 7.1 SAD of AgPt phase; the satellite spots are most likely generated by spinodal decomposition; however more diffraction studies are required.....	44
Figure 7.2 Simulated $[100]$ zone axis diffraction pattern of AgPt, calculated by using a FePt $L1_0$ unit cell, which was modified for AgPt with lattice parameters adjusted to $a = 0.42 \text{ nm}$ and $c = 0.40 \text{ nm}$ ²⁷	45
Figure 7.3 SAD pattern of AgPt showing closely spaced satellite spots on either side of the main spots. The satellite spots are most likely due to a composition modulation such as spinodal decomposition.....	46
Figure 7.4 Simulated $[101]$ zone axis diffraction pattern of AgPt, calculated by using a FePt $L1_0$ unit cell, which was modified for AgPt with lattice parameters adjusted to $a = 0.42 \text{ nm}$ and $c = 0.40 \text{ nm}$ ²⁷ . This zone axis is the best match for Fig. 7.3.	46
Figure 7.5 Simulated structure for AgPt $L1_1$ based on CuPt $L1_1$ structure ²⁷	47

Figure 7.6 Simulated unit cell for AgPt L1₀ structure; adapted from FePt L1₀²⁷48

Figure 7.7 Simulated AgPt L1₀ structure adapted from FePt L1₀²⁷49

LIST OF TABLES

Table 2.1 Comparison of calculated and measured composition values for liquidus temperatures.....11

LIST OF ABBREVIATIONS

BSE	Backscattered electron
DSC	Differential Scanning Calorimetry
DTA	Differential Thermal Analysis
EDS	Energy Dispersive X-ray Spectroscopy
EMPA	Electron Microprobe Analysis
FCC	Face Centred Cubic
FEG	Field Emission Gun
FIB	Focused Ion Beam
LRO	Long Range Order
MD	Molecular Dynamics
SAD	Selected Area Diffraction
SEM	Scanning Electron Microscopy
SRO	Short Range Order
TEM	Transmission Electron Microscopy
XRD	X-ray Diffraction
PIPS	Precision Ion Polishing System

1 INTRODUCTION

1.1 BACKGROUND

The demand for new materials has resulted in widespread use of computational tools to theoretically predict materials which have outstanding properties. These predictions should be validated by experimental investigations. If this is not done the predictions are of limited usefulness in service. Equiatomic silver-platinum (AgPt) is one such material. It has been predicted to have the $L1_1$ ordered structure¹ which has only previously been observed in Cu-Pt alloys and may have exceptional mechanical properties. The research presented here aims to establish, experimentally, the nature of the equiatomic phase in the Ag-Pt alloy system.

1.2 THE SILVER-PLATINUM ALLOY SYSTEM

The earliest work on this system dates back to the 1800s². It is thus a system that has been studied for hundreds of years, but the results remain inconclusive. The reason for this is that silver and platinum are expected to form a solid solution of silver in platinum (and *vice versa*) because both are FCC in crystal structure. Silver and platinum, however, are immiscible in the solid state across most of the compositional range, with a limited solubility of platinum in silver and a minimal solubility of silver in platinum. In order to produce the most recent phase diagram, Durussel and Feschotte³ heat treated alloys for 200 days at 300°C, 150 days at 500°C and 100 days at 800°C to achieve equilibrium structures: an indication that the kinetics of phase formation is sluggish in this system.

This dissertation describes the result of heat treating Ag-Pt alloys for up to 80 days. The heat treated alloys were investigated by Energy Dispersive X-ray Spectroscopy (EDS), Scanning Electron Microscopy (SEM) and Transmission Electron Microscopy (TEM). Specimens were also investigated using Differential Scanning Calorimetry (DSC) as well as hardness measurements.

1.3 OBJECTIVES

The objectives of this research are to:

- Confirm the presence of an ordered phase at or near the equiatomic composition in the Ag-Pt system
- Determine the structure of the ordered phase
- Evaluate the equiatomic region of the most recent phase diagram.

1.4 LIMITATIONS AND SCOPE OF THESIS

The major limitation of this research was the long heat treatments that needed to be conducted in order to prepare reproducible samples. The alloy was not homogenized after cold rolling which could have been the reason for the long heat treatments. The heat treatments were carried out for 20 to 80 days.

1.5 PLAN OF DEVELOPMENT

An extensive literature review conducted on published work on the Ag-Pt system is presented in Chapter 2. This is followed by a description of experimental procedures in Chapter 3, succeeded by results and preliminary discussion in Chapter 4. A discussion highlighting the most important results is then given in Chapter 5 followed by conclusions in Chapter 6. Recommendations are made for future research in Chapter 7 based on the conclusions; and a list of references is given in Chapter 8.

2 LITERATURE REVIEW

2.1 THE SILVER-PLATINUM SYSTEM: PREVIOUS EXPERIMENTAL WORK

The Ag-Pt system has been the topic of discussion for more than 100 years. The earliest work on the Ag-Pt system was published in 1867 by Matthiessen², who studied the electrical properties of the alloy across the entire composition range. He found an anomaly in the composition-property curves at \approx Ag 22 at.% Pt. However, he did not consider this to be sufficient basis for assuming the existence of a phase change in the region.

In 1906, Thompson and Miller⁴ studied the microstructure and electrical properties of Ag-Pt alloys containing up to 43 at.% Pt. After quenching Ag 20 at.% Pt in cold water from the molten state, they observed a second phase, which persisted when the platinum content was increased to 25 at.% Pt and the alloy was slow cooled from the molten state. They noted from hardness, electrical resistance and specific gravity measurements that the values of these properties increased as the platinum content increased, reaching a maximum at Ag 43 at.% Pt, which the authors explained by postulating the presence of a chemical compound in that composition region.

The first equilibrium phase diagram to be constructed was by Doerinckel⁵ in 1907, who carried out a systematic study across the entire Ag-Pt composition range as shown in Fig. 2.1.1. When the platinum concentration was increased to above 36 at.% Pt, there was a dramatic change in the microstructure with the appearance of a second phase. This phase was identified as the chemical compound Ag_2Pt .

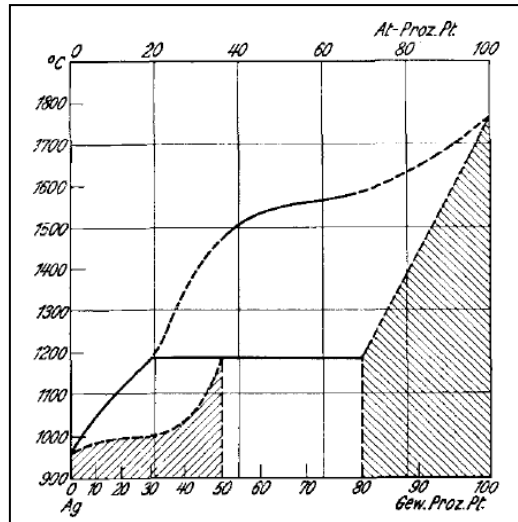


Figure 2.1.1 Phase diagram for the Ag-Pt system, after Doerinckel ⁵.

In 1927, Kurnakow and Nemilow⁶ studied electrical conductivity, hardness, limit of tensile strength and microstructure across the entire Ag-Pt composition range. They amended Doerinckel's data⁵ and made the limits of solubility of the components more precise, as shown in Fig. 2.1.2. According to their data, the maximum solubility of platinum in silver is ≈ 36 at.% Pt, and of silver in platinum, ≈ 12 at.% Ag. In relation to the change in the properties studied, they concluded that there are no chemical compounds formed in this system.

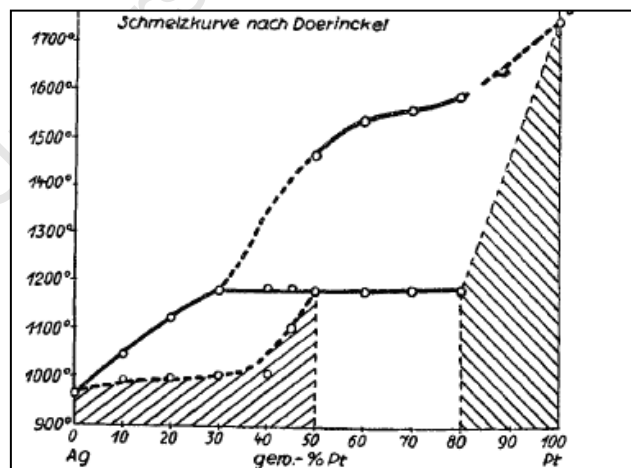


Figure 2.1.2 Phase diagram for the Ag-Pt system, after Kurnakow and Nemilow⁶.

In 1930, Johansson and Linde⁷ studied the crystal structure, electrical resistivity and thermal conductivity of Ag-Pt alloys heat treated at different temperatures. From Fig.

2.1.3, the local minimum in electrical resistivity observed at ≈ 50 at.% Pt is a clear indication of ordering⁸.

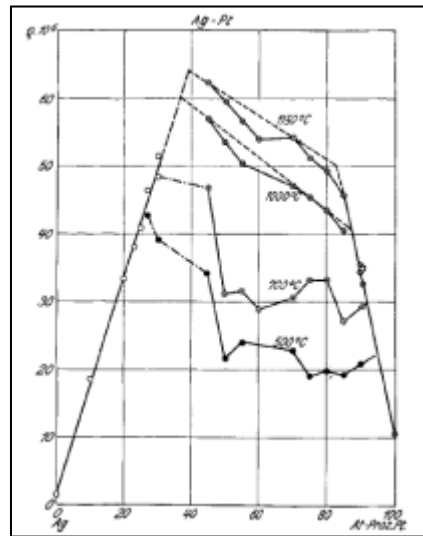


Figure 2.1.3 Graph showing electrical resistivity vs composition of Ag-Pt alloys at different temperatures, after Johansson and Linde⁷.

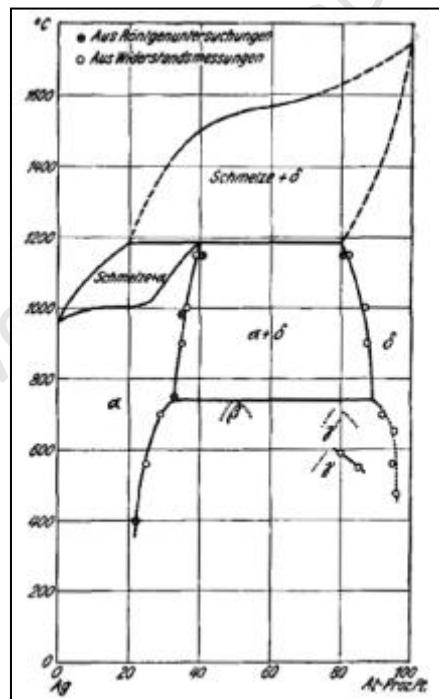


Figure 2.1.4 Phase diagram for the Ag-Pt system, after Johansson and Linde⁷ (● – Electrical resistivity measurements, ○ – X-ray diffraction measurements).

Using electrical resistivity data and X-ray diffraction results, Johansson and Linde⁷ constructed the phase diagram in Fig. 2.1.4. They identified two new phases that are

unstable above 750°C, i.e. AgPt (β phase) and AgPt₃ (γ and γ'). They suggested that the β phase might have the same ordered structure as AuCu, PdCu and PtCu. They concluded that the phase diagram by Doerinckel⁵ was correct. They also found that below 750°C there is a miscibility gap and that there might be three or four ordered structures in that region.

In 1943, Schneider and Esch⁹ repeated Johansson and Linde⁷'s experiments but they only focused on the temperature range 685-1130°C. They found three compounds: Ag₃Pt in the form of two modifications (α and α'), AgPt (β phase), AgPt₃ also in the form of two modifications (γ and γ') and a new phase in the region of 90 at% Pt.

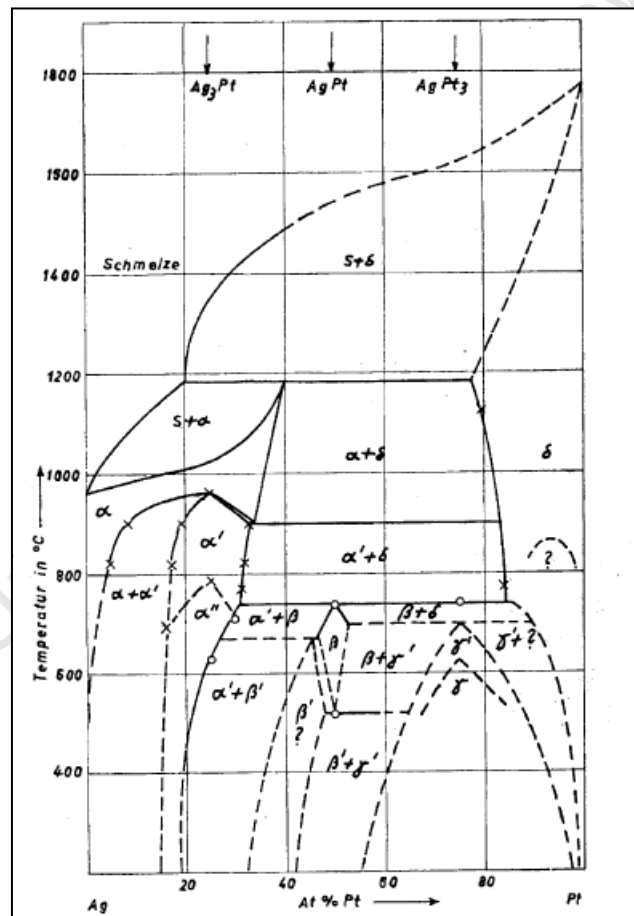


Figure 2.1.5 Phase diagram for the Ag-Pt system, after Schneider and Esch⁹ (X - X-ray crystallographic measurements and o - conductivity measurements).

According to Novikova and Rudnitskii¹⁰, the two works described above^{7, 9} are inconclusive and the changes in resistivity could be explained by the non-equilibrated state of the alloys rather than by the appearance of new phases. In order to demonstrate this, they studied the hardness, microstructure, electrical resistance and temperature coefficients of resistivity of Ag-Pt alloys across the entire composition range. They also performed X-ray diffraction on all the alloys that they prepared and the results were used to plot the following phase diagram.

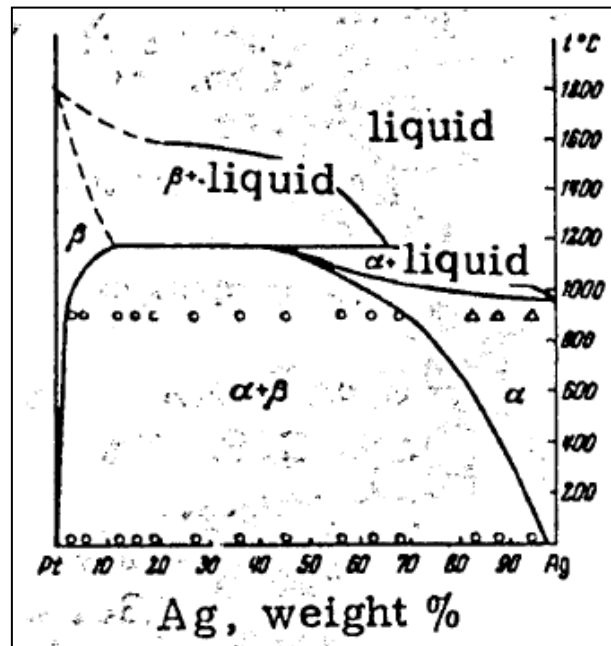


Figure 2.1.6 Phase diagram for the Ag-Pt system, after Novikova and Rudnitskii¹⁰.

From the phase diagram above, Novikova and Rudnitskii¹⁰ ruled out any low temperature structures. Their results showed almost complete immiscibility across the entire compositional range at 900°C.

Klement and Luo¹¹ found that by rapidly quenching alloys from the melt a continuous solid solution is formed, but at equilibrium the FCC components form a peritectic system. They fabricated their alloys by using powdered silver and platinum pressed into compacts and sintered at 1000°C in a hydrogen atmosphere for at least 16 hours then furnace cooled. Owing to the inhomogeneity of alloys with ≈ 40 at.% Pt, the sintered compacts were induction melted under hydrogen then cold rolled into

wires. After heating small pieces of the alloys to $\approx 50^\circ\text{C}$ above the liquidus, the molten alloy was ejected by a blast of helium onto a copper strip on a rotating wheel. This method of splat cooling produced flakes that were $\approx 1\text{mm}^2$ in area.

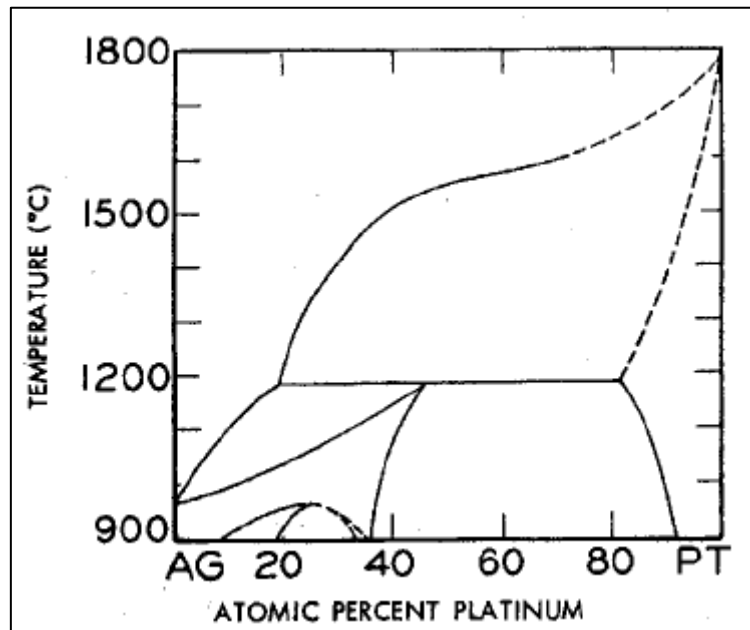


Figure 2.1.7 Revised phase diagram for the Ag-Pt system, after Klement and Luo⁹.

Klement and Luo used information from Hansen and Anderko¹² as well as from Novikova and Rudnitskii¹⁰ to produce the equilibrium phase diagram in Fig. 2.1.7. Klement and Luo produced non-equilibrium solid solutions from rapidly solidified alloys. They performed X-ray diffraction and measured the lattice parameters for comparison with the previous results by Schneider and Esch⁹, Johannsen and Linde⁷, and Novikova and Rudnitskii¹⁰. From Fig. 2.1.8 it is clear that their measurements agree well with the previous work.

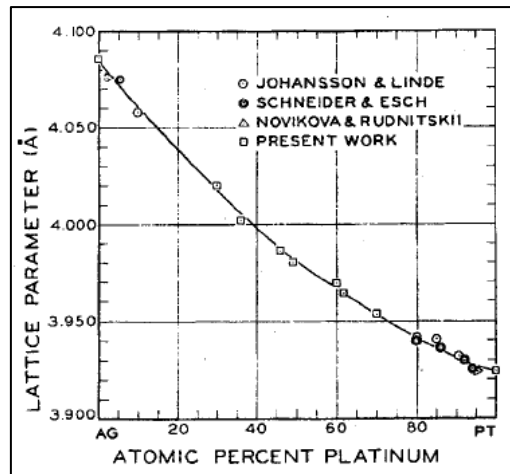


Figure 2.1.8 Lattice parameters of FCC solid solutions in Ag-Pt alloys¹¹.

Ebert *et al.*¹³ agreed that although the Ag-Pt system obeys the Hume-Rothery rules, it possesses limited solubility. They noted that the solubility over the entire composition range can only be extended by quenching from the melt at a high cooling rate as Klement and Luo¹¹ did. They used a different type of splat cooling called a gun technique which incorporates a pressure pulse of duration about 1 μ s during the impact of the molten droplet on the substrate. This leads to further effective supercooling of the melt because the equilibrium phase diagram is strongly influenced by the change in pressure¹³. Ebert *et al.*¹³ found that alloys containing up to 10 at.% Pt and more than 94 at.% Pt were single phase. The alloys with concentrations in between these boundaries, from 10 at.% Pt to 94 at.% Pt, were splat cooled and X-ray diffraction patterns were used to determine the lattice parameters. Their lattice parameter measurements agree with previous measurements^{7, 9-11}.

The most recent experimental phase diagram is by Durussel and Feschotte³. They revised the existing phase diagrams by using Differential Thermal Analysis (DTA), X-ray Diffraction (XRD) and Electron Microprobe Analysis (EMPA). Only one ordered phase, with chemical formula $\text{Ag}_{15}\text{Pt}_{17}$, was detected at 53 ± 0.5 at.% Pt. The phase is reported to be stable below 803°C but the composition range of existence is very narrow. XRD has confirmed that there are two-phase regions at 52 and 54 at.% Pt.

The composition and the narrow region of existence of this phase were confirmed by EMPA measurements and micrographs³.

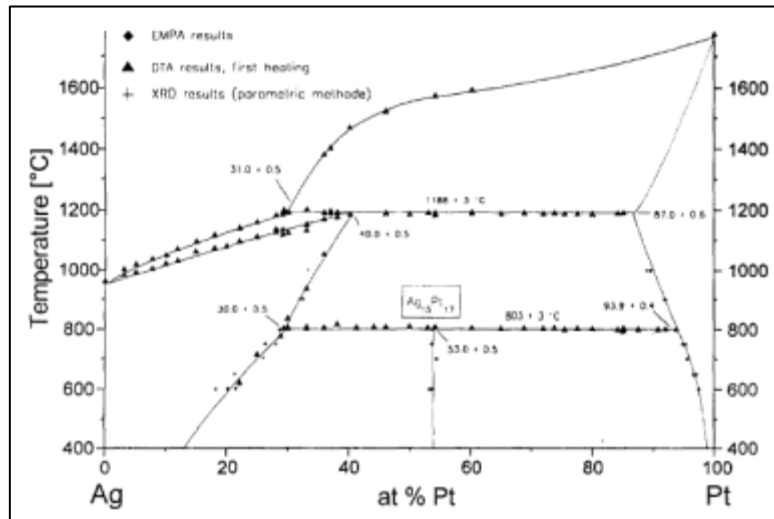


Figure 2.1.9 The most recent Ag-Pt phase diagram, after Durussel and Feschotte³.

Durussel and Feschotte³ annealed the experimental alloys for 200 days at 300°C, 150 days at 500°C and 100 days at 800°C in order to obtain reproducible results for the peritectic transformations as well as the ordered region. The crystal structure of the near-equiatomic alloy could not be determined, but XRD suggested that the $\text{Ag}_{15}\text{Pt}_{17}$ has a deformed cubic structure corresponding to a 32 atom unit cell.

Erni *et al.*¹⁴ investigated the proposed L_{12} ordered Ag_3Pt phase. According to Schneider and Esch⁹ and Karakaya and Thompson¹⁵, this L_{12} phase is stable below 770°C. Erni *et al.*¹⁴'s alloys were prepared in an arc-furnace, then homogenised in a cold-crucible levitation furnace at an increased pressure. Thereafter, alloys were cast into rods and the rods were swaged to 3 mm then aged for 12 and 40 days at 770°C. The rods were cut into discs and prepared for Transmission Electron Microscopy (TEM). The TEM results show that there are no extra reflections in the expected positions for the L_{12} superstructure. They concluded that there is no tendency toward order and that the Ag_3Pt structure is not present at low temperatures. These results agree with Durussel and Feschotte³ as well as Novikova and Rudnitskii¹⁰.

2.2 COMPUTATIONAL PREDICTIONS OF ORDERING IN THE SILVER-PLATINUM SYSTEM

Karakaya and Thompson¹⁵ partially calculated the Ag-Pt phase diagram by thermodynamic modelling of the liquid phase and solid solutions to obtain the phase boundaries. They presumed that the alloy would have a solid solution across the entire composition range because of the FCC structure of silver and platinum, but they concluded from their calculations that a miscibility gap forms. The Gibbs energy for the different phases was calculated separately and each equation took into account the enthalpies and entropies of mixing. Some of the results calculated by Karakaya and Thompson⁹ are compared to Doerinckel's⁵ experimental results in Table 2.1, showing the accuracy of their calculations.

Table 2.1 Comparison of calculated and measured composition values for liquidus temperatures.

Temperature (°C)	Calculated (at.% Pt) ¹⁵	Measured (at.% Pt) ⁵
990	1.4	...
1045	5.6	5.8
1120	13.3	12.2
1181	19.7	19.2
1463	36	35.7
1535	45.5	45.5
1559	52.5	56.5
1588	69.4	69

The results above show that the liquidus compositions measured experimentally by Doerinckel⁵ in 1907 are consistent with the liquidus that was calculated by Karakaya and Thompson¹⁵ 80 years later. The assessed phase diagram shows both calculated and experimentally measured results by these authors.

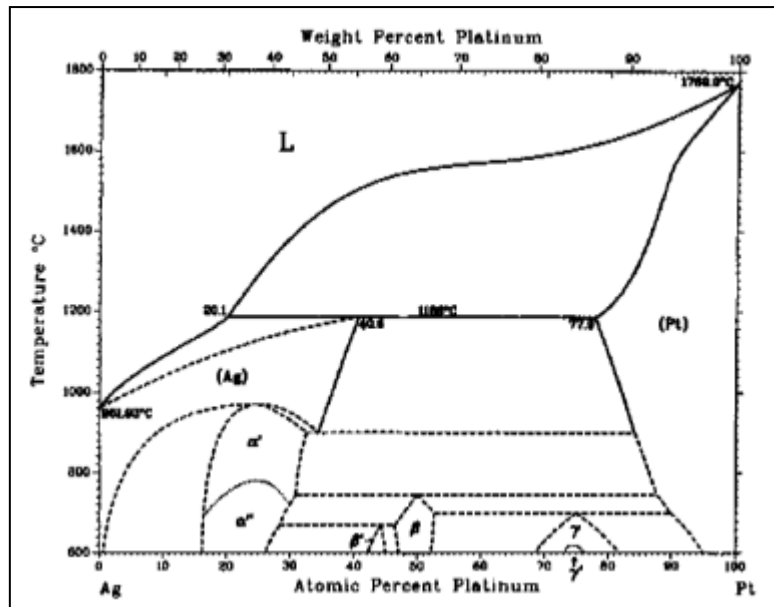


Figure 2.2.1 Assessed phase diagram for the Ag-Pt system, by Karakaya and Thompson¹⁵.

The phase boundaries shown by the solid lines on the phase diagram in Fig. 2.2.1 are based on thermodynamic modelling by Karakaya and Thompson¹⁵ whereas the dashed lines are associated with intermetallics after Hansen¹². Hansen¹² predicts a β phase at the 50:50 composition but he does not have a structure for it. There is a number of intermetallics predicted for the lower part of the phase diagram shown in figure 2.2.1. Karakaya and Thompson¹⁵ concluded that a complete systematic experimental study is required to resolve the uncertainties surrounding the intermetallic phases.

Takizawa *et al.*¹⁶ analysed the phase stability of nine binary alloy systems including Ag-Pt. They calculated the heats of formation by performing local-density-functional band calculations. It was found that the relativistic effect plays a crucial role in phase stability of platinum based alloys. In heavy elements like platinum, the 6s orbital is pulled closer to the nucleus by the relativistic effect. This shifts the s band downward in energy resulting in an increase of d holes and thus an enhancement of the d -band cohesion. This implies that the attractive interaction between platinum atoms may be strong enough for platinum to segregate in alloys¹⁶. To confirm the relativistic effect, Takizawa *et al.*¹⁶ calculated the heats of formation with relativistic corrections and without. Their results are shown overleaf:

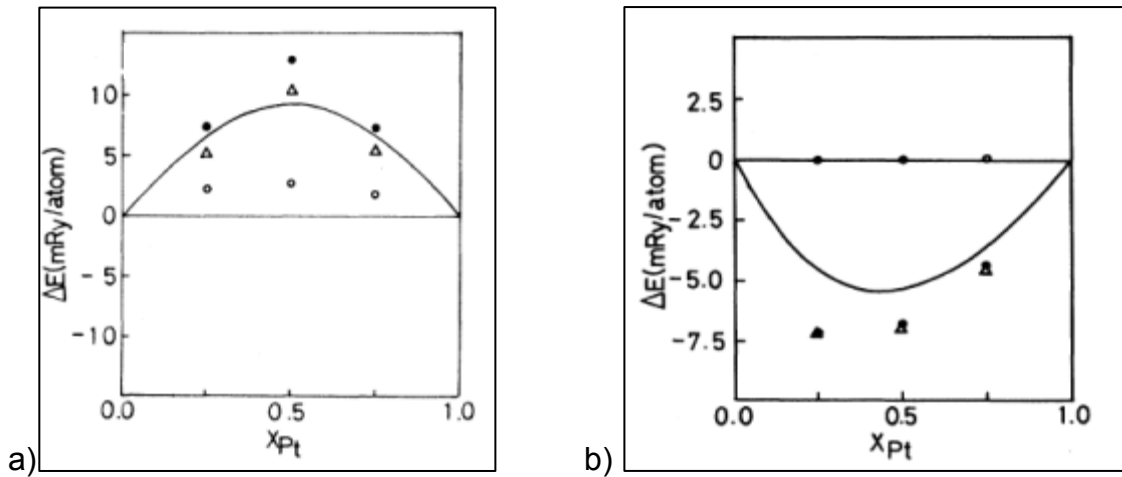


Figure 2.2.2 a) Calculated heats of formation with relativistic correction and b) Calculated heats of formation without relativistic correction¹⁶.

From the diagrams above it is evident that the relativistic effect plays an important role in alloy formation in the Ag-Pt system. Takizawa *et al.*¹⁶ concluded that the Ag-Pt system is a complicated system but they also predicted that the $L1_1$ structure forms at low temperatures. They encouraged experimental verification of that prediction because the $L1_1$ structure has been thought to be unique to the Cu-Pt system.

The $L1_1$ structure is a superlattice with the elements alternating along $[111]$; it has been described¹⁷ as a deformed cubic structure. Durussel and Feschotte³ could not make a single crystal to determine the exact structure of the $Ag_{15}Pt_{17}$ phase but they could determine that the structure was deformed cubic with 32 atoms in the unit cell.

Sluiter *et al.*¹⁸ performed *ab initio* calculations of phase stability in Au-Pd and Ag-Pt alloys. They noted that the Ag-Pt system displays peculiar behaviour; although the formation enthalpies are positive for the majority of the studied structures, a few structures display negative formation enthalpies¹⁸. According to their ground state calculations (Fig. 2.2.3), only a single intermetallic is predicted to be stable, at the equiatomic composition with the $L1_1$ structure.

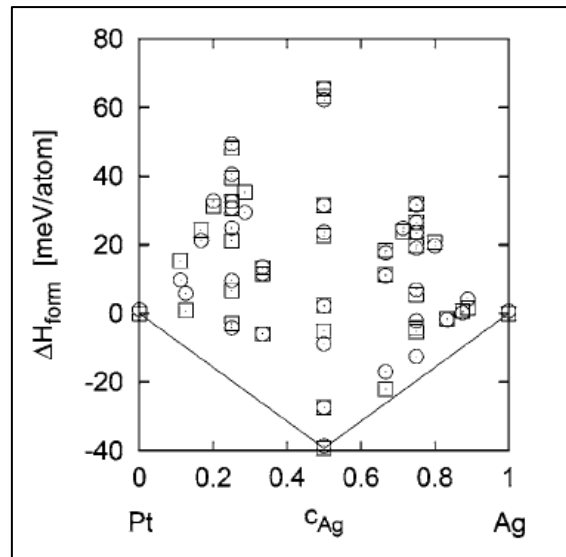


Figure 2.2.3 Formation enthalpies of ordered structures in the Ag-Pt system¹⁸.

The following phase diagram was calculated using two different methods¹⁸ in which the nearest neighbours and cluster expansion terms were varied to produce the phase diagram which shows the $L1_1$ forming in a narrow region. Decomposition occurs through a peritectoid reaction, at about 1000K (727°C) which is not in agreement with the experimental value of 1076K (803°C). The miscibility gap and the line compound are the only similarities to the phase diagram by Durussel and Feschotte³.

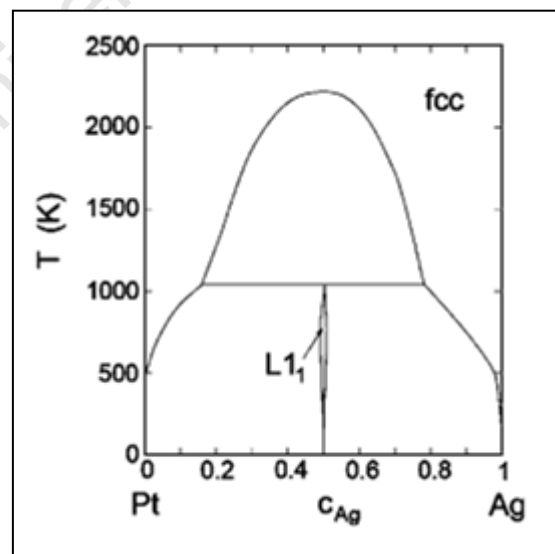


Figure 2.2.4 Computed phase diagram for the Ag-Pt system¹⁸.

Sluiter *et al.*¹⁸ concluded that Ag-Pt exhibits ordering exclusively for structures with $\langle \frac{1}{2} \frac{1}{2} \frac{1}{2} \rangle$ type ordering wave vectors and probably at the equiatomic composition only; whereas at higher temperatures a miscibility gap exists in the FCC solid solution. They also found that the $L1_1$ structure is the only stable compound at ambient temperature and that the $Ag_{15}Pt_{17}$ structure proposed by Durussel and Feschotte³ appears to be closely related to the $L1_1$ structure.

In 2011 Yan *et al.*¹⁹ investigated the Finnis-Sinclair potentials for the Au-Pd and Ag-Pt systems. The Finnis-Sinclair potential is an embedded atom potential that incorporates the band character of metallic cohesions and allows calculation of correct values for vacancy formation and cohesive energy²⁰. These calculations are used to describe atomic interactions. The alloys were studied using a molecular dynamics (MD) simulation that predicts the thermal and mechanical properties of the alloys. The temperature dependence of lattice constants, cohesive energies, elastic constants, bulk modulus and melting temperatures for some Au-Pd and Ag-Pt alloys were predicted for the first time using MD simulations. Yan *et al.*¹⁹ found that as the temperature increases, lattice constant increases whereas cohesive energy decreases from 0–900K. The predictions were compared to available experimental data and the data for pure Ag and pure Pt.

Nelson *et al.*¹ investigated systems predicted to exhibit $L1_1$ and $L1_3$ crystal structures as low temperature ground state structures. The results for the Ag-Pt system are shown below:

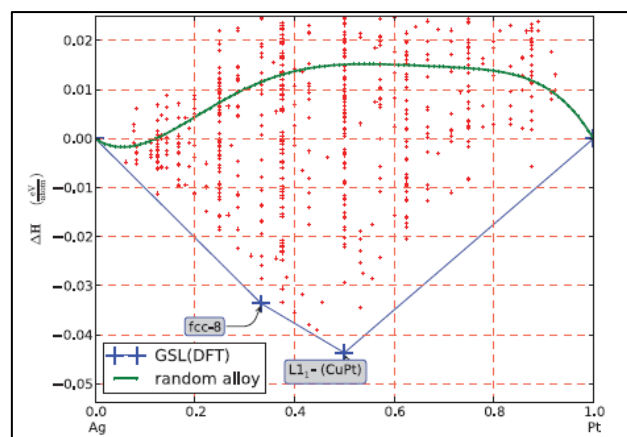


Figure 2.2.5 Low temperature ground states for the Ag-Pt system¹.

First principles calculations for the ground states found for the system differ from the experimental phases mentioned above. From Figure 2.2.5, Ag_2Pt (fcc-8) and AgPt (L1_1) are stable by first principle methods. The phase with structure fcc-8 is an AB2 stacking in the [111] direction of a FCC lattice. The most recent experimental phase diagram by Durussel and Feschotte³ reports an ordered phase with composition $\text{Ag}_{15}\text{Pt}_{17}$. Nelson *et al.*¹ searched all 32 atoms/cell configurations but yielded no ground state at 15:17 stoichiometry. The 32-atom cell with the lowest formation energy was very similar to the L1_1 structure. Nelson *et al.*¹ assumes that the reported phase was in fact L1_1 with a small number of random defects, or that the experimental determination of the composition was incorrect. Monte Carlo simulations executed for the 1:1 composition indicate a transition temperature of $\approx 700^\circ\text{C}$, which is inconsistent with the experimental transition temperature of the ordered phase (β) reported by Schneider and Esch⁹ as well as the transition temperature of 803°C for the $\text{Ag}_{15}\text{Pt}_{17}$ phase by Durussel and Feschotte³.

2.3 ORDERING

In a binary solid solution the two atomic species can arrange themselves in a number of different ways¹⁷. The atoms can either have a random or ordered configuration depending on the temperature of the alloy. Thermodynamically stable ordered phases, sometimes called intermediate or intermetallic compounds, form at or near compositions corresponding to a simple ratio of components such as AB or AB₂. If the structure only exists at an exact ratio, it is known as a line compound¹⁷.

At low temperatures thermal vibrations and thermal motion are at a minimum; this is where ordering easily occurs¹⁷. The process involves a change from a statistically nearly random distribution of A and B atoms in a crystal lattice to a more regular arrangement. This regular arrangement is characterised by the preference for either like or unlike nearest neighbours²¹. The chemical nature of the atoms will dictate the energetically favoured bonds that would form; that is, like or unlike nearest neighbours may be favoured but not both simultaneously²². For a disordered alloy of composition AB, either one of the atoms A or B can occupy any point on the lattice. Once ordering has occurred, the A and B atoms start to rearrange, with each atom preferring a certain lattice position. The resulting arrangement can be described as a lattice of A atoms interpenetrating a lattice of B atoms. This segregation may occur with little or no deformation and the resulting lattice is referred to as a superlattice or a superstructure¹⁷.

Figure 2.3.1 shows a disordered phase as well as a superlattice of copper and gold atoms in the ratio 3:1 (Cu₃Au). In the disordered phase the copper and gold atoms can occupy any of the atomic sites as long as the ratio of gold to copper atoms remains 1:3 according to the stoichiometric formula, as shown in Fig. 2.3.1 (a). Figure 2.3.1 (b) shows an example of gold atoms interpenetrating a lattice of copper atoms to form the L1₂ superlattice¹⁷.

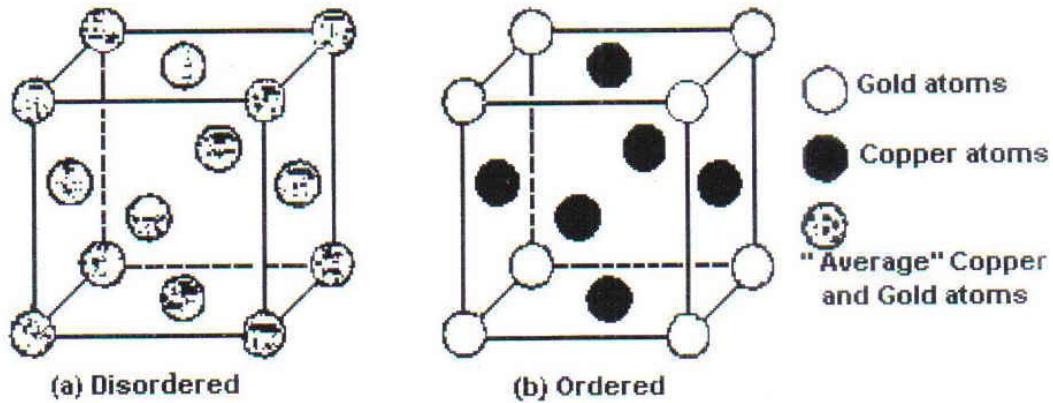


Figure 2.3.1 (a) An example of a disordered copper-gold lattice and (b) The ordered structure of Cu_3Au (L1_2)¹⁷.

The formation of a superlattice can be described as Long Range Order (LRO), which occurs at low temperatures and at stoichiometric compositions such as AB_3 , AB or compositions close to these. There is a critical temperature, T_c , below which ordering starts to take place. Above T_c the configuration is random and as the temperature is lowered below T_c the degree of ordering increases towards perfection¹⁷.

Another type of ordering that may exist above T_c is Short Range Order (SRO). This type of ordering is not dependent on T_c and occurs at temperatures below or above T_c for alloys that have a tendency to form LRO¹⁷. In some systems, SRO is a precursor to LRO.

2.4 THE L₁ ORDERED STRUCTURE

In the Cu-Pt system at the equiatomic composition, as temperature decreases through T_c , the disordered lattice transforms to form the L₁ ordered structure. The L₁ structure is described as alternating layers of Cu and Pt atoms on (111) planes¹⁷. This form of ordering produces a lattice distortion from cubic to rhombohedral for which the Strukturbericht designation is L₁. CuPt is the only experimentally known example of this structure²³.

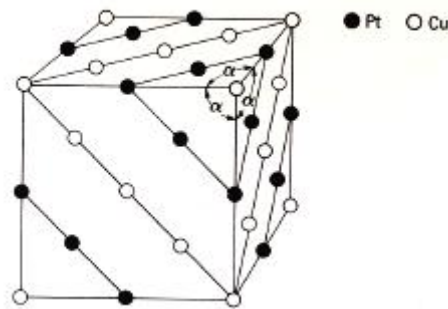


Figure 2.4.1 Distribution of atoms at the composition CuPt showing the alternate (111) planes that are occupied by Cu and Pt atoms¹⁷.

The ordered rhombohedral unit cell has a lattice parameter of $2a$ (8 atoms in an FCC unit cell) as compared to the primitive unit cell of FCC lattice with lattice parameter a (1 atom per cell)²⁴.

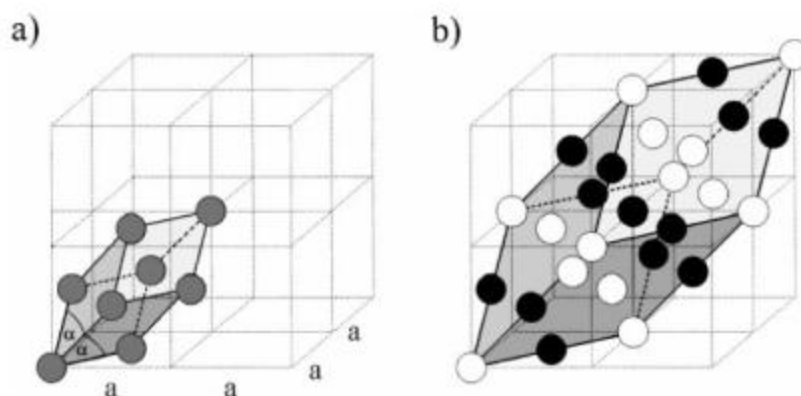


Figure 2.4.2 (a) Primitive unit cell for FCC-lattice with lattice parameter a (disordered state). (b) Ordered rhombohedral unit cell of CuPt with new lattice parameter $2a$ ²⁴.

The first image in figure 2.4.2 overleaf is actually a cubic unit cell. The reason it is shown at an angle is to emphasise the distortion that takes place on ordering shown in (b), although somewhat exaggerated in the figures shown. The ordered lattice is double the original lattice parameter and there are alternating layers of either Cu or Pt atoms on [111] planes.

Recently, Nelson *et al.*¹ showed that there are many systems that are predicted to possess the $L1_1$ structure as a ground state structure. The reason for the apparent absence of this structure may be due to the low temperature at which this structure appears for many systems.

University of Cape Town

3 EXPERIMENTAL PROCEDURES

3.1 ALLOY PREPARATION

Two alloys were studied experimentally. The first alloy was made at the Centre for Materials Engineering using a *Hot Platinum ICON 3CS* induction casting machine. The second alloy was made by Perkins Metal Recoveries using silver and platinum granules. EDS determined the compositions to be Ag 54±1 at.% Pt and Ag 51±1 at.% Pt respectively. The alloys were not homogenised prior to or post cold rolling so the initial alloys were inhomogenous .

3.2 SPECIMEN PREPARATION

The buttons were rolled to 90% reduction in thickness using a *Dinkel* laboratory rolling mill. The strip of metal that was produced was then cut in squares of approximately 1 cm x 1 cm using a *Buehler Isomet* low speed saw with a diamond blade for SEM and hardness measurements. Self-supporting discs 3mm in diameter with a thickness of 350–420µm were punched from the rolled alloy for DSC and TEM analysis.

3.3 HEAT TREATMENTS

Before any of the heat treatments were conducted, the samples were coated with Isomol, a ceramic paste, to prevent oxidation at elevated temperatures. The heat treatments were carried out in muffle furnaces for 20, 40, 60 and 80 days at 750°C terminated by quenching into water. This temperature was chosen because it is well below the transformation temperature according to Durussel and Feschotte³.

3.4 METALLOGRAPHY

3.4.1. GRINDING

Prior to grinding, all 1 cm x 1 cm samples were mounted in a transparent acrylic hot mounting resin, using a *Struers Labopress-3*. The mounted samples were then ground on a *Struers Labopol-25* grinding machine using 1200 grit grinding paper to

create a smooth, flat surface. Mounted specimens were then placed in a beaker containing ethanol and placed in an ultrasonic bath for a minute to remove any surface impurities; thereafter they were dried with a heat dryer.

3.4.2. POLISHING

A *Metaserve C200/5V* universal polisher was used to polish the samples. Three μm diamond paste (DP mol), 1 μm diamond paste (DP flocc) and $\frac{1}{4}$ μm diamond paste (DP nap) polishing pads were used for all samples. All samples were cleaned in ethanol in an ultrasonic bath between polishing pads, to remove the diamond paste and lubricant used previously.

3.5 HARDNESS

The 1 cm x 1 cm specimens were prepared as detailed in 3.4 above. The microhardness tests were performed using the *Highwood HWDM-3* microhardness tester. The Vickers diamond indenter was used with a load of 100gf and dwell time of 10 seconds.

3.6 DIFFERENTIAL SCANNING CALORIMETRY (DSC)

Durussel and Feschotte³ did Differential Thermal Analysis (DTA) measurements to find the transformation temperature of their ordered phase.

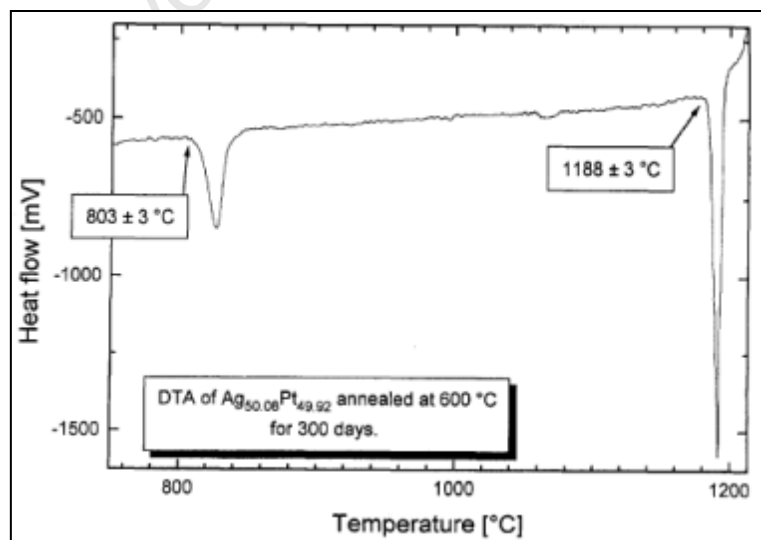


Figure 3.6.1 DTA of $\text{Ag}_{50.08}\text{Pt}_{49.92}$ annealed at 600°C for 300 days³.

The difference between DSC and DTA is that DTA measures temperature difference between a sample and an inert reference (usually Al_2O_3) while heat flow to the reference and the sample remains the same, while DSC measures differences in the amount of heat required to increase the temperature of a sample and a reference as a function of temperature²⁵. Both show a transformation temperature but they are measured differently; nevertheless they showing the same results and therefore they can be compared directly.

A *Netzsch STA409* thermal analyser was used, fitted with an S-type thermocouple, with a maximum operating temperature capability of 1500°C . The samples for DSC were 3 mm punched discs that were approximately 20 mg in mass. An alumina (Al_2O_3) crucible was used, with a lid, in both the reference and sample positions. The temperature profile was: room temperature to 900°C at a heating rate of $15^\circ\text{C}/\text{min}$, followed by an isothermal holding time of 15 minutes, and finally a cool down from 900°C to room temperature at a cooling rate of $15^\circ\text{C}/\text{min}$. The specific heating and cooling rates were selected to allow sufficient time for transformation whilst maintaining the ability to resolve the differential between the sample and the reference. The heating curves of heat flow vs temperature were plotted, and the endothermic peaks were analysed by determining peak onset temperature, maximum peak temperature and peak area.

3.7 SCANNING ELECTRON MICROSCOPY (SEM)

An *FEI Nova™ NanoSEM 230* scanning electron microscope (SEM) was used with a 20 kV accelerating voltage. Backscattered electron (BSE) images were obtained using the SEM. The only sample preparation required was a mounted and polished 1 cm x 1 cm surface, prepared as described above in 3.4.3.

3.7.1 ENERGY DISPERSIVE X-RAY SPECTROSCOPY (EDS)

The SEM was equipped with a spectrometer able to detect X-rays emitted by the specimen during electron beam excitation. These X-rays hold a typical energy and wavelength which when measured reveal the elemental composition of an area. A common type of X-ray analysis used in conjunction with an SEM is Energy

Dispersive Spectroscopy (EDS). EDS was utilised in order to analyse the composition of the phases that were present in the alloy. The analysis software was Inca and spot/point analyses were used, together with elemental area mapping. This is a semi-quantitative analysis which means that it is approximately correlated instead of precision driven with a 1% error in the measurements.

3.7.2 FOCUSED ION BEAM (FIB)

An *FEI Helios Nanolab 650* equipped with a FIB and SEM (FIB SEM) operating from 500 V to 30 kV making use of FEI's *Duelbeam™* platform, was used for preparing a 50 µm TEM specimen from the area of interest.

3.8 TRANSMISSION ELECTRON MICROSCOPY (TEM)

The 3mm discs were ground using 1200 grit SiC paper, from 350 µm to 100 µm thickness using water as a lubricant. The specimens were dimpled using *Gatan* dimpler to reduce the thickness of the centre of the discs from 100 µm to 30 µm. A *Gatan Precision Ion Polishing System* (PIPS) was used to mill the specimens to perforation. The milling used argon gas and operated at an accelerating voltage of 5 kV. The ion guns were set at varying angles between 3° and 6°. Perforation occurred at three to five hours.

A *Philips TECNAI TF20* electron microscope, equipped with a Field Emission Gun (FEG) as the electron source was used at an operating voltage of 200kV. This microscope is housed in the Electron Microscope Unit at UCT.

A *JEOL JEM-ARM 200F* electron microscope, also equipped with a FEG, was used at an operating voltage of 200kV. This microscope has an improved resolution compared to the Tecnai due to C_s correction and therefore clearer high magnification images were obtainable. This microscope is housed in the Centre for High Resolution Transmission Electron Microscopy at Nelson Mandela Metropolitan University.

4 RESULTS

4.1 THE EFFECT OF HEAT TREATMENT ON MICROSTRUCTURE

The effect of heat treatment on microstructure was evaluated for the following alloys: Ag 54±1 at.% Pt and Ag 51±1 at.% Pt. An SEM with backscattered electron (BSE) detector was used for the images because it shows differences in atomic number as different intensities or shades. The element with the highest atomic number appears the brightest in a BSE image; in this case platinum, as it has an atomic number of 78 whereas silver has an atomic number of 47 and thus appears darker. This was helpful in identifying visually the different phases that are present in the alloys. The compositional analyses were carried out by EDS at 20 spots across the entire specimen and the averages are shown with 1% error.

4.1.1 AS-CAST

Figure 4.1.1 shows the cast Ag 54±1 at.% Pt alloy showing a dendritic microstructure. This indicates that there was a compositional variation which was confirmed by the compositional analysis. This shows that there is a Pt-rich phase coexisting with an Ag-rich phase as shown in figure 4.1.1.

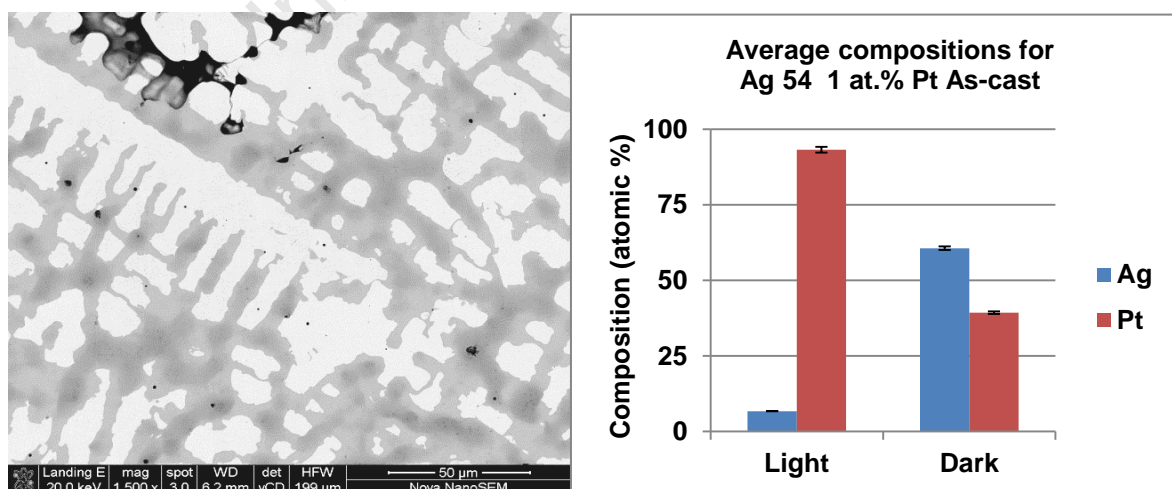


Figure 4.1.1 BSE micrograph and compositional analysis of Ag 54±1 at.% Pt as-cast.

Figure 4.1.2 shows the cast microstructure for Ag 51±1 at.% Pt, also showing dendritic growth but instead of the two phases seen in Figure 4.1.1, there were three phases evident. The light phase has composition of Ag 63±1 at.% Pt, the dark phase is Ag 22±1 at.% Pt and the new, grey phase is Ag 42±1 at.% Pt.

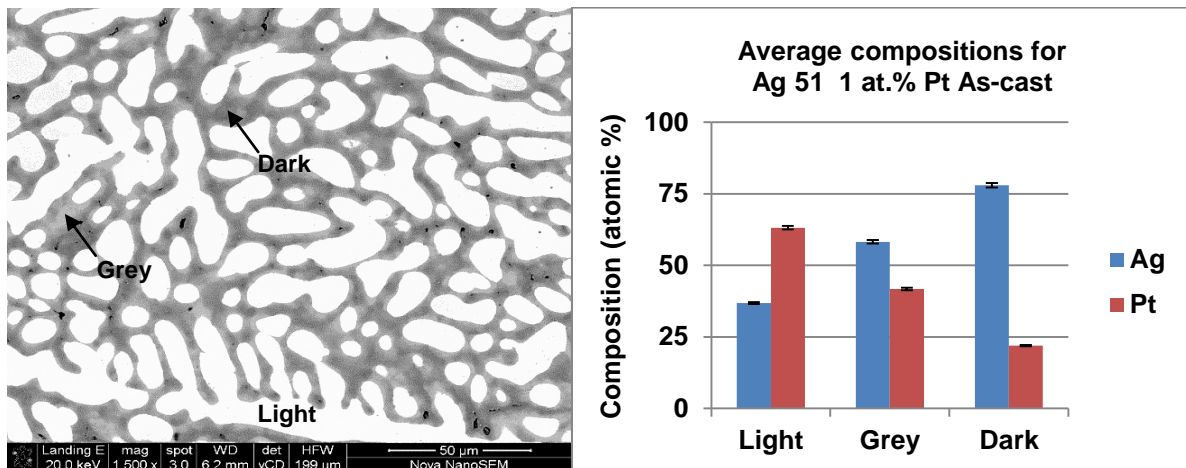


Figure 4.1.2 BSE micrograph and compositional analysis of Ag 51±1 at.% Pt as-cast.

4.1.2 20 DAYS AT 750°C

The rolled alloy was placed in a furnace at 750°C for 20 days, after which the Ag 54±1 at.% Pt alloy was still two-phase with a slight change in the compositions of the light and dark phases, as shown in Figure 4.1.3.

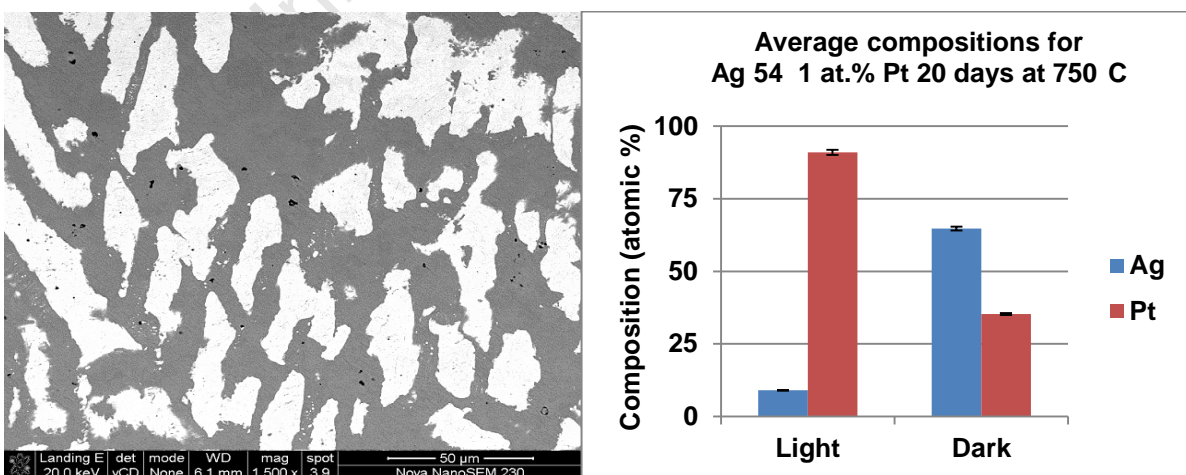


Figure 4.1.3 BSE micrograph and compositional analysis of Ag 54±1 at.% Pt after 20 days at 750°C.

The Ag 51±1 at.% Pt alloy, which started with three phases, showed an increase in volume fraction of the third phase after 20 days at 750°C. The composition of this third (grey) phase is approximately Ag 52±1 at.% Pt, as shown in Figure 4.1.4.

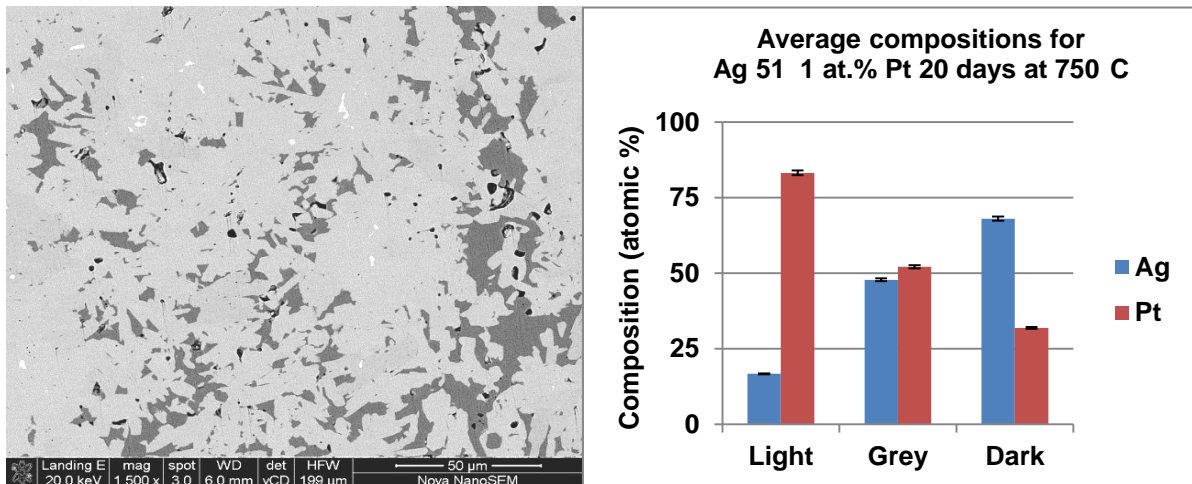


Figure 4.1.4 BSE micrograph and compositional analysis of Ag 51±1 at.% Pt after 20 days at 750°C.

4.1.3 40 DAYS AT 750°C

After 40 days at 750°C, a third phase emerges in the Ag 54±1 at.% Pt alloy, as shown in Figure 4.1.5 below. This third (grey) phase has the same composition, Ag 52±1 at.% Pt, as seen in Figure 4.1.4 above.

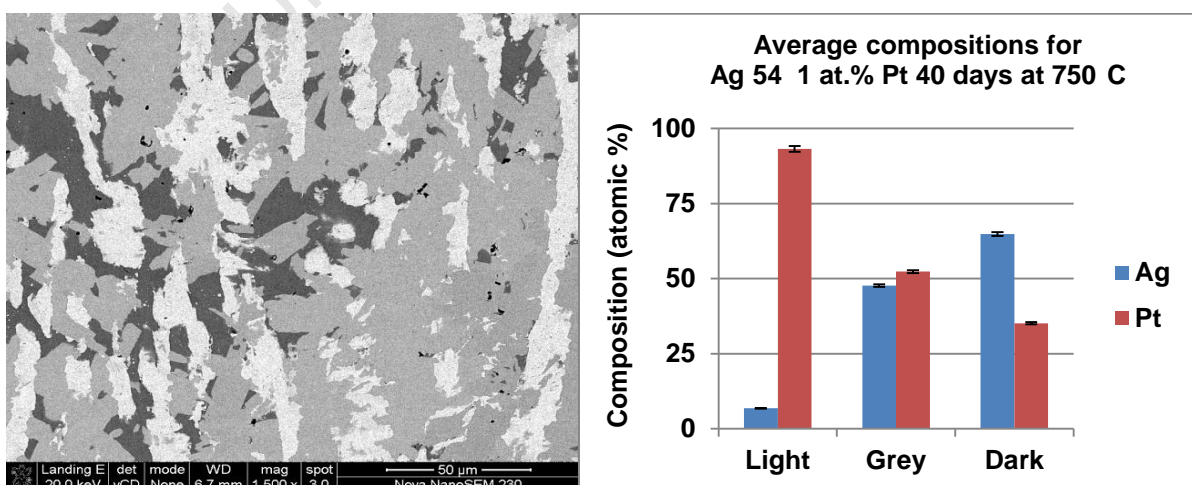


Figure 4.1.5 BSE micrograph and compositional analysis of Ag 54±1 at.% Pt after 40 days at 750°C.

After 40 days at 750°C, the grey phase of the Ag 51±1 at.% Pt alloy continues to increase in volume fraction until the dark and light phase are barely visible, as shown in Figure 4.1.6.

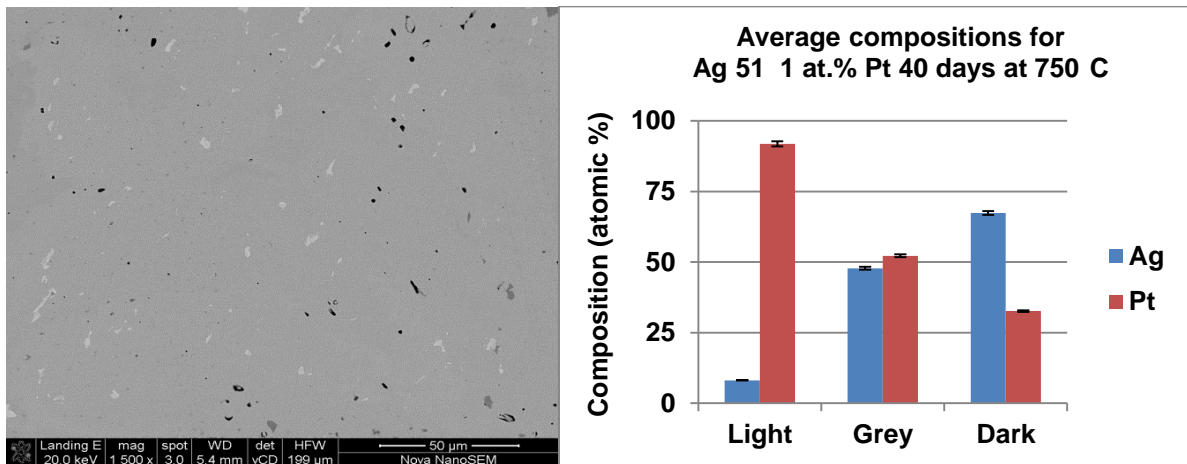


Figure 4.1.6 BSE micrograph and compositional analysis of Ag 51±1 at.% Pt after 40 days at 750°C.

4.1.4 60 DAYS AT 750°C

The Ag 54±1 at.% Pt alloy still has three phases after 60 days at 750°C, with a slight increase in the volume fraction of the third (grey) phase. The composition of this grey phase is still around Ag 52±1 at.% Pt, as seen in Figure 4.1.7.

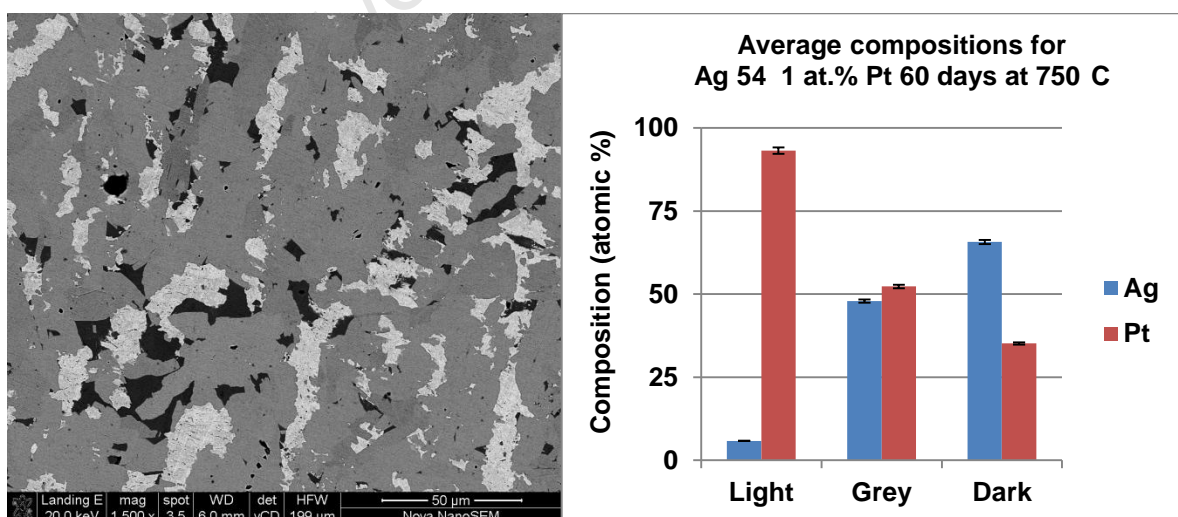


Figure 4.1.7 BSE micrograph and compositional analysis of Ag 54±1 at.% Pt after 60 days at 750°C.

The following images were taken in order to have a 3-D image of the specimen. These images show the distribution of the third phase and the growth pattern. It shows that the third phase does not have a preferred growth orientation, and is randomly distributed throughout the specimen.

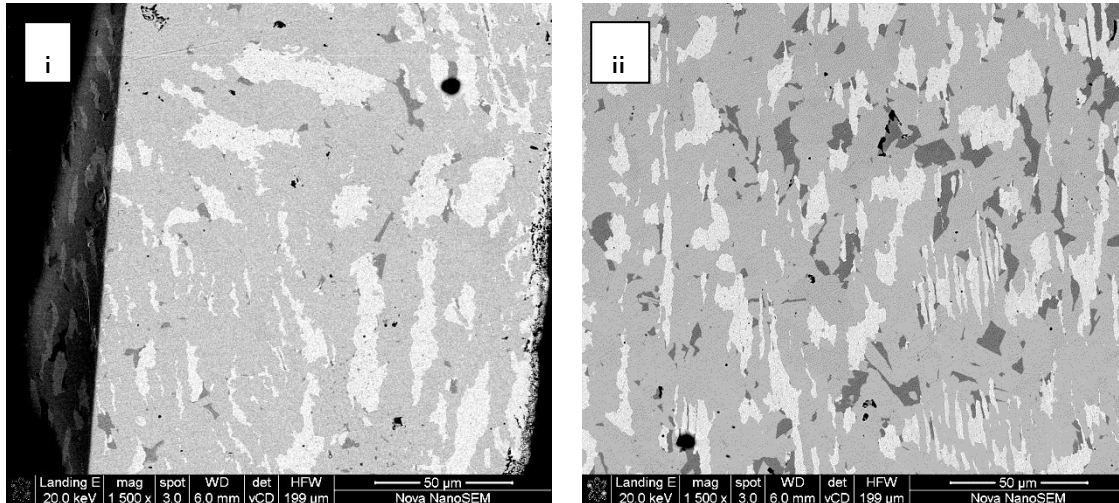


Figure 4.1.7 (i) Transverse cross section BSE micrograph of Ag 54±1 at.% Pt after 60 days at 750°C; (ii) Longitudinal cross section of Ag 54±1 at.% Pt after 60 days at 750°C.

In Figure 4.1.8, the volume fraction of the third phase in Ag 51±1 at.% Pt appears to be continuing to increase. The composition of the third phase is Ag 53±1 at.% Pt. This is the same composition as the line compound by Durussel and Feschotte³.

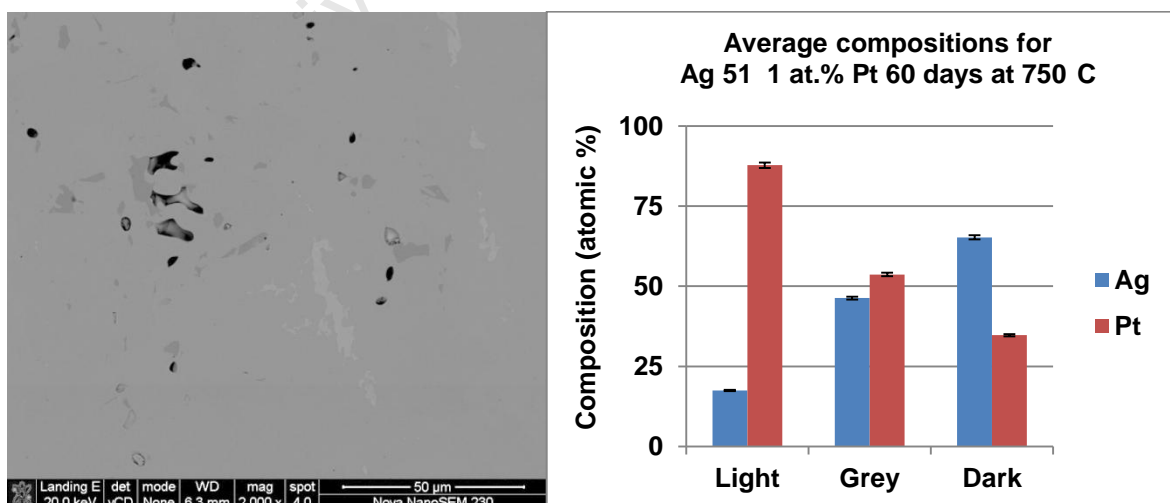


Figure 4.1.8 BSE micrograph and compositional analysis of Ag 51±1 at.% Pt after 60 days at 750°C.

4.1.5 80 DAYS AT 750°C

The volume fraction of the third phase in Ag 54±1 at.% Pt, as shown in Figure 4.1.9, was expected to be higher after 80 days at 750°C. Instead it looks more like Figure 4.1.5; i.e. the third phase appears to have reduced.

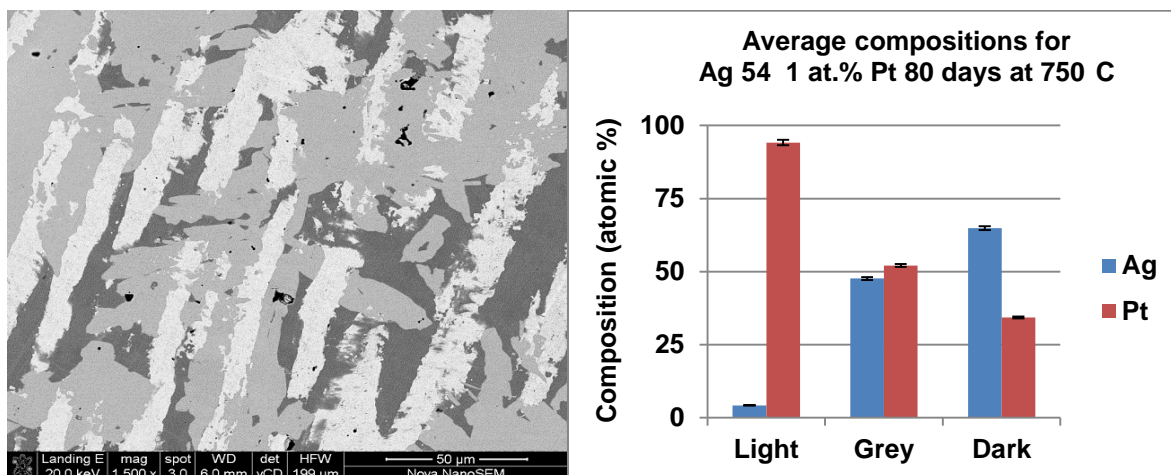


Figure 4.1.9 BSE micrograph and compositional analysis of Ag 54±1 at.% Pt after 80 days at 750°C.

Figure 4.1.10 shows Ag 51±1 at.% Pt, which as expected has a higher volume fraction of the third phase after 80 days at 750°C. The composition of the third phase in Figure 4.1.10 is Ag 52±1 at.% Pt.

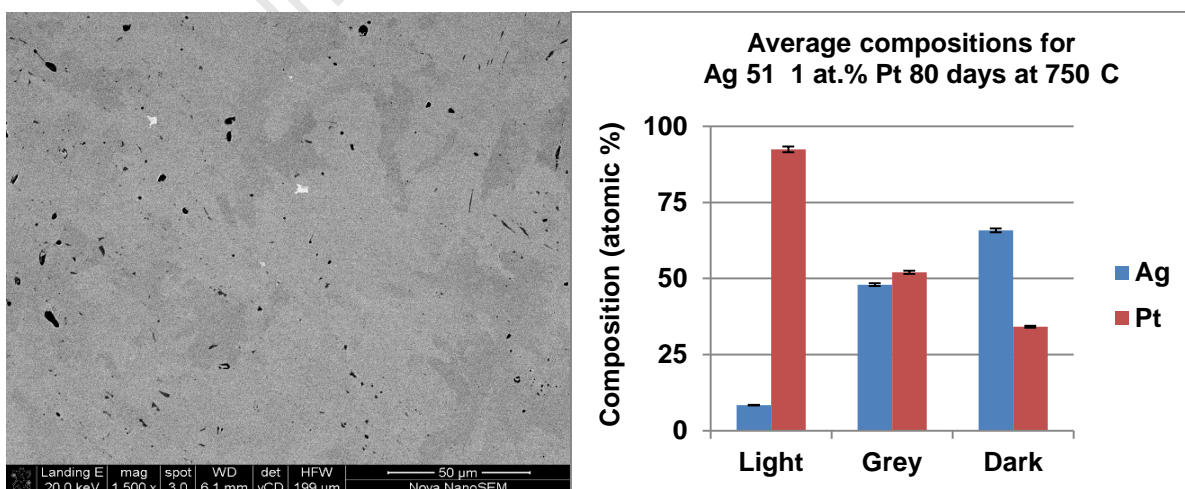


Figure 4.1.10 BSE micrograph and compositional analysis of Ag 51±1 at.% Pt after 80 days at 750°C.

4.1.6 40 DAYS AT 850°C

The reason for this heat treatment was to validate the transformation temperature of 803°C, shown in the phase diagram in Figure 2.1.9. From Figure 4.1.11 and 4.1.12 it is clear that after heat treatment there are only two phases present, a silver-rich phase and a platinum-rich phase; the “third” phase is no longer evident.

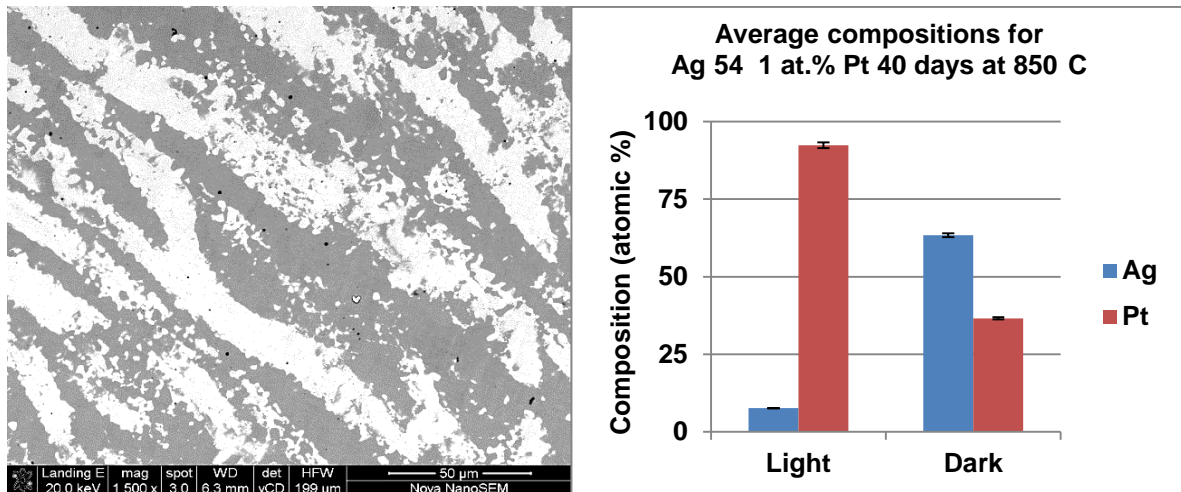


Figure 4.1.11 BSE micrograph and compositional analysis of Ag 54±1 at.% Pt after 40 days at 850°C.

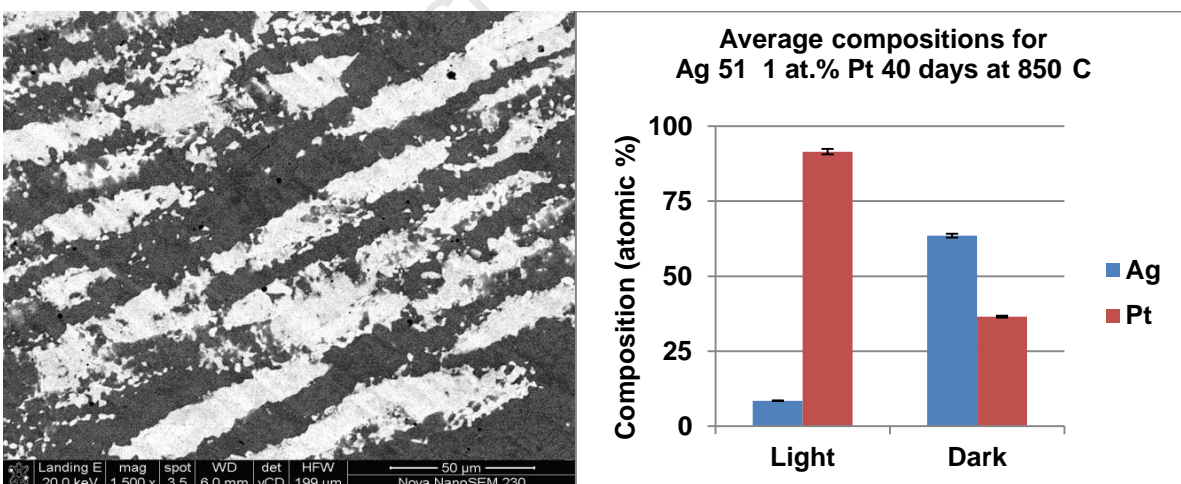


Figure 4.1.12 BSE micrograph and compositional analysis of Ag 51±1 at.% Pt after 40 days at 850°C.

4.2 THE EFFECT OF HEAT TREATMENT ON HARDNESS

An increase in hardness after heat treatment may indicate the development of ordering in many systems²². From Figure 4.2.1 it is evident that the hardness increases after heat treatment of both as-cast alloys, and continues to increase as the number of days at 750°C increases. After 80 days the hardness is even higher. There is a decrease in hardness after 40 days at 850°C, which is above the transformation temperature, to the same hardness as the cast structure. Given that there are cold-worked microstructures, the onset of recrystallisation could also lead to drastic reduction in hardness. However, there is no evidence in the studied microstructures to suggest that recrystallisation has played a role.

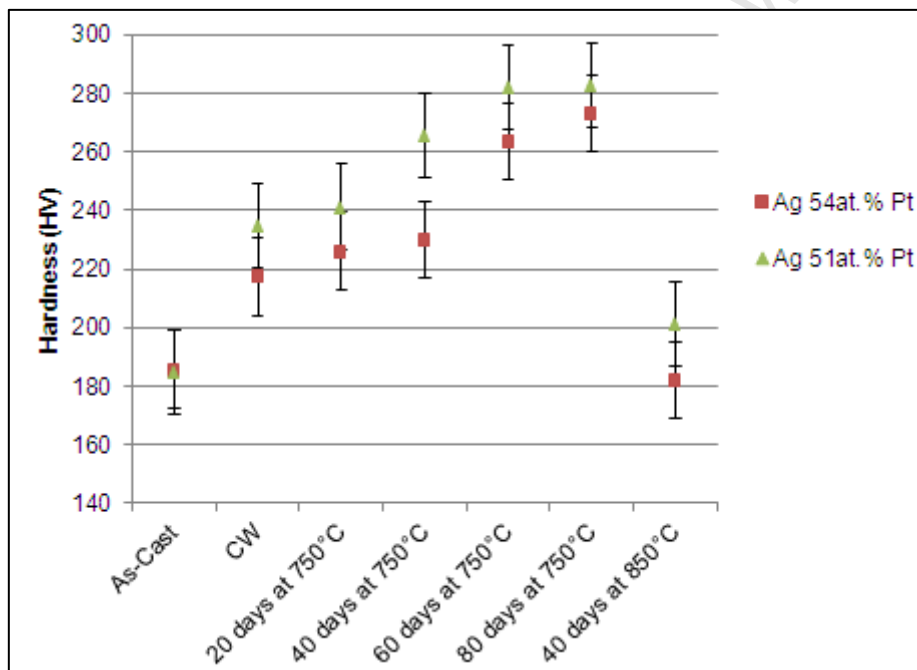


Figure 4.2.1 Vickers hardness of alloys showing an increase in hardness at 750°C and decrease in hardness at 850°C.

4.3 DISSOLUTION TEMPERATURES USING DSC

The DSC measurements were carried out in order to identify the dissolution temperature of the third phase, which was no longer observed after heat treatment at 850°C.

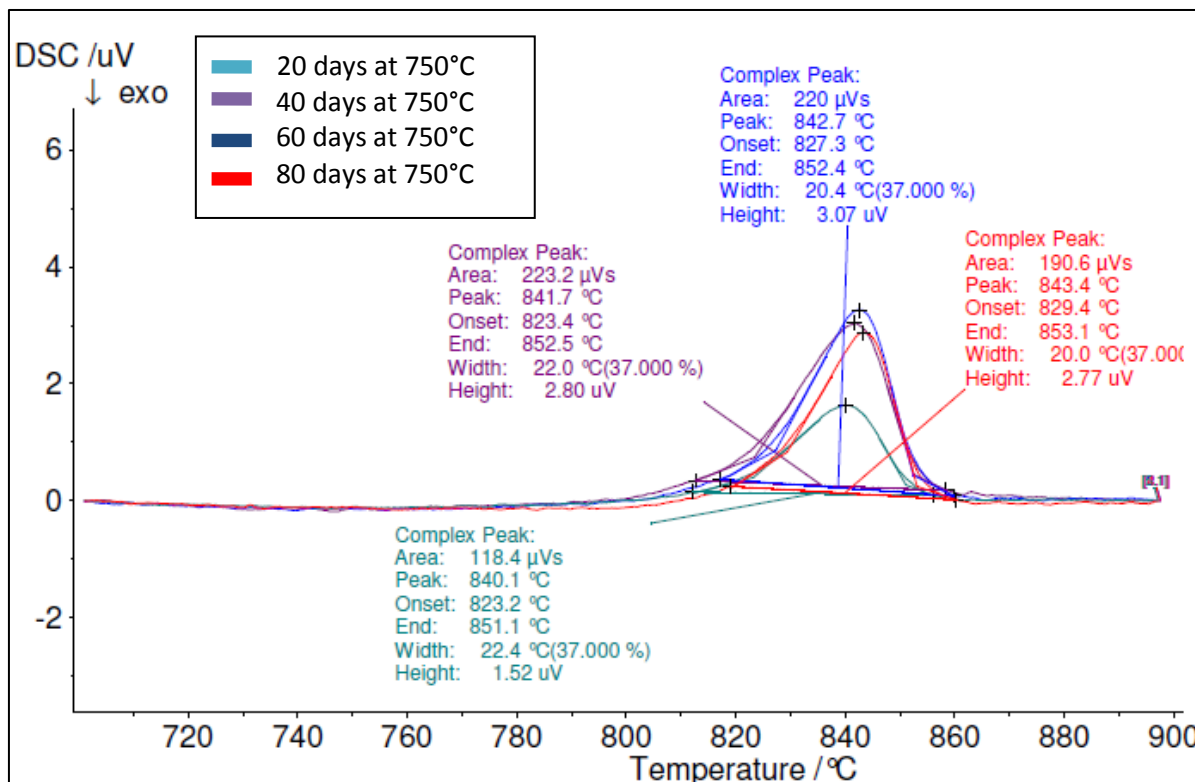


Figure 4.3.1 DSC results for Ag 54±1 at.% Pt

Figure 4.3.1 shows the DSC curves for Ag 54±1 at.% Pt, which show endothermic peaks above 800°C. These peaks show an onset temperature (on heating) of 823-829°C with a variation of $\pm 5^{\circ}\text{C}$.

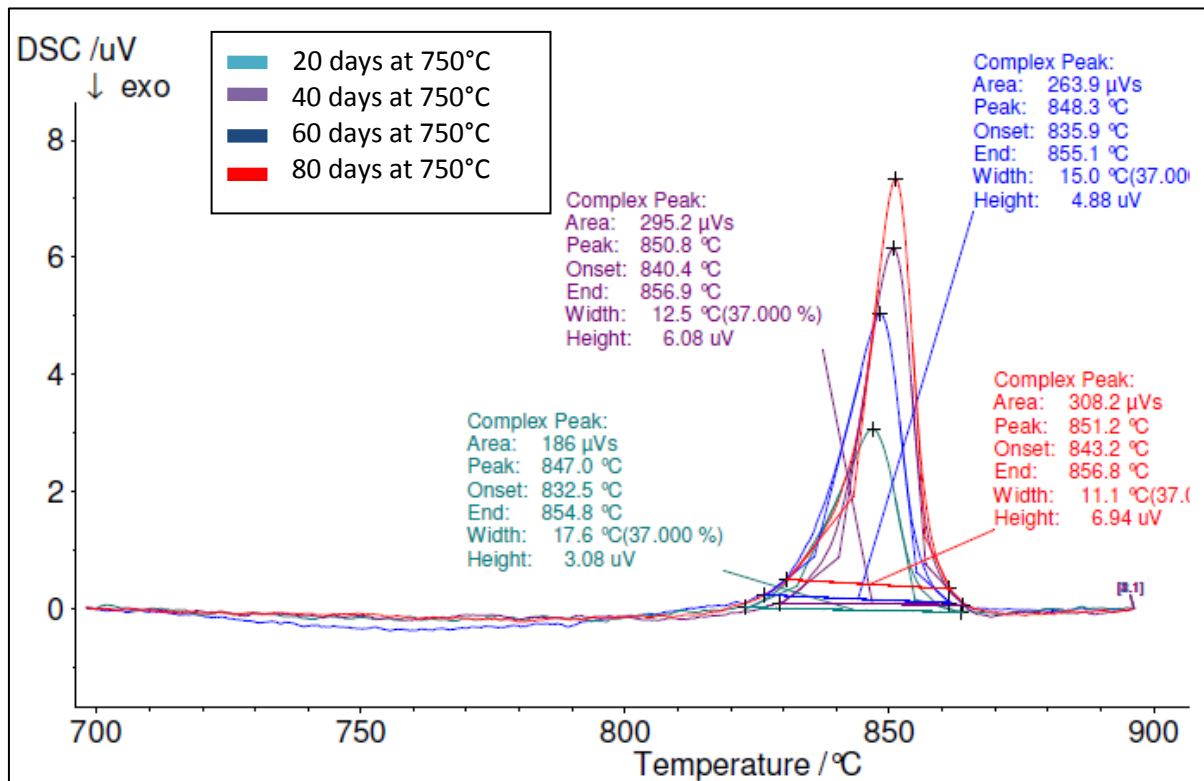


Figure 4.3.2 DSC results for Ag 51 \pm 1 at.% Pt

Figure 4.3.2 shows the DSC curves for Ag 51 \pm 1 at.% Pt, which also show endothermic peaks way above 800 $^{\circ}\text{C}$. These onset temperatures are higher than those seen for the Ag 54 \pm 1 at.% Pt alloy: from 832-843 $^{\circ}\text{C}$ with a variation of \pm 10 $^{\circ}\text{C}$.

4.4 CRYSTAL STRUCTURE ANALYSIS USING ELECTRON DIFFRACTION

In section 4.2 it was shown that the hardness increased as time at 750°C increased. A possible reason could be that a phase transformation had taken place. An electron diffraction study was carried out to investigate this in both alloys.

The electron diffraction patterns shown in Figure 4.4.1 and 4.4.2 below were obtained from cold rolled samples of both alloys. Owing to the two-phased nature of the alloy, one cannot be sure which phase is represented in the diffraction patterns. It is most definitely either a solid solution of Ag in Pt or vice versa. The diffraction pattern only shows the fundamental reflections associated with the $[100]_{\text{fcc}}$ zone axis.

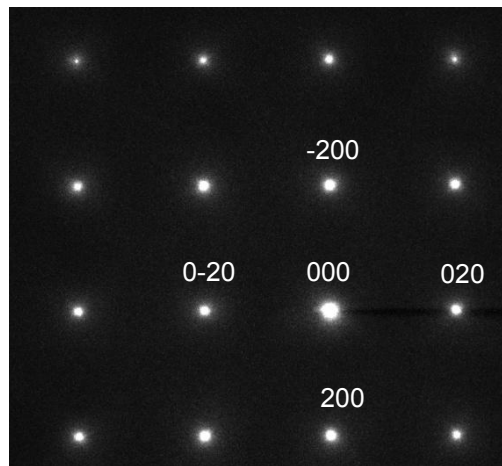


Figure 4.4.1 Electron diffraction pattern for cold rolled Ag 54±1 at.% Pt, viewed along the $[100]_{\text{fcc}}$ zone axis.

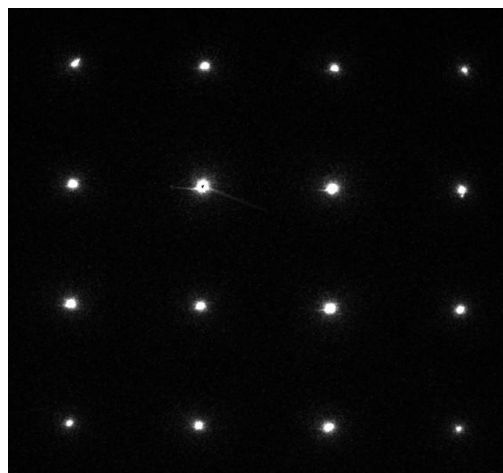


Figure 4.4.2 Electron diffraction pattern for cold rolled Ag 51±1 at.% Pt, viewed along the $[100]_{\text{fcc}}$ zone axis.

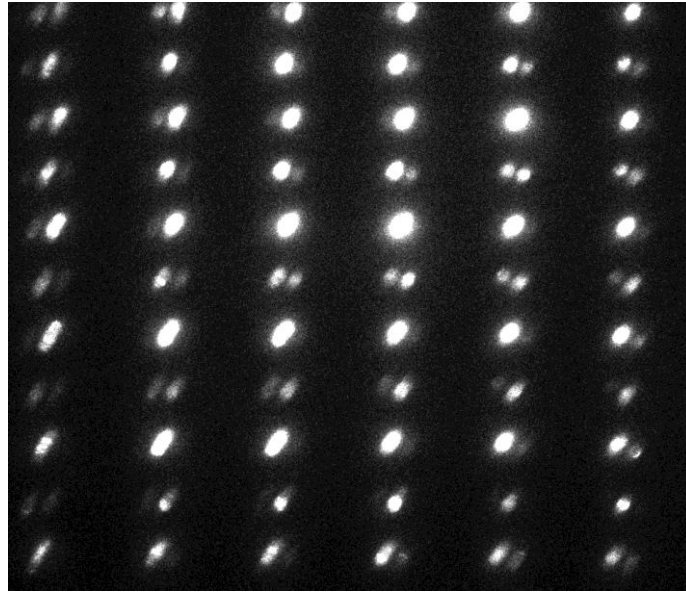


Figure 4.4.3 Electron diffraction pattern for Ag 51 ± 1 at.% Pt, heat treated at 750°C for 80 days, possibly viewed along the $[100]_{\text{fcc}}$ zone axis.

After heat treatment at 750°C , specimens of each alloy were prepared for electron microscopy. Electron diffraction shows additional doublet spots halfway between the fundamental reflections, as shown in Figure 4.4.3. This is definitely the third phase because the solid solutions of Ag in Pt or Pt in Ag would show distinct FCC spots. Dark field images suggest that the presence of the third phase observed by SEM is responsible for these multiple reflections but only part of the edge of the specimen is seen in bright contrast probably due to specimen bending and/or thickness changes in the foil.

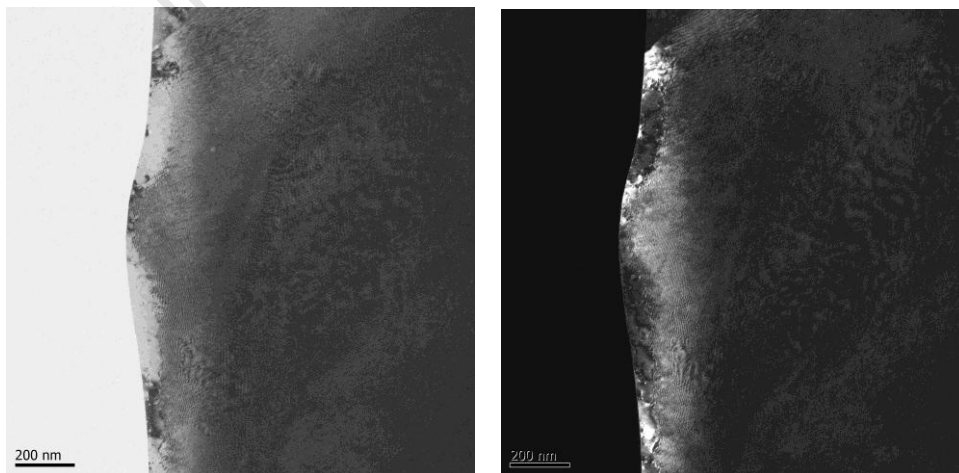


Figure 4.4.4 Bright field (left) and dark field (right) pair obtained using additional reflection in Figure 4.4.3.

The specimen shown in Figs 4.4.3 and 4.4.4 was prepared for TEM using a PIPS ion mill. The possibility of artefacts from specimen preparation led to a change in technique. A further set of electron diffraction patterns was obtained, this time from specimens prepared using a FIB SEM. Again, multiple extra reflections were observed in the electron diffraction patterns, as shown in Figure 4.4.5.

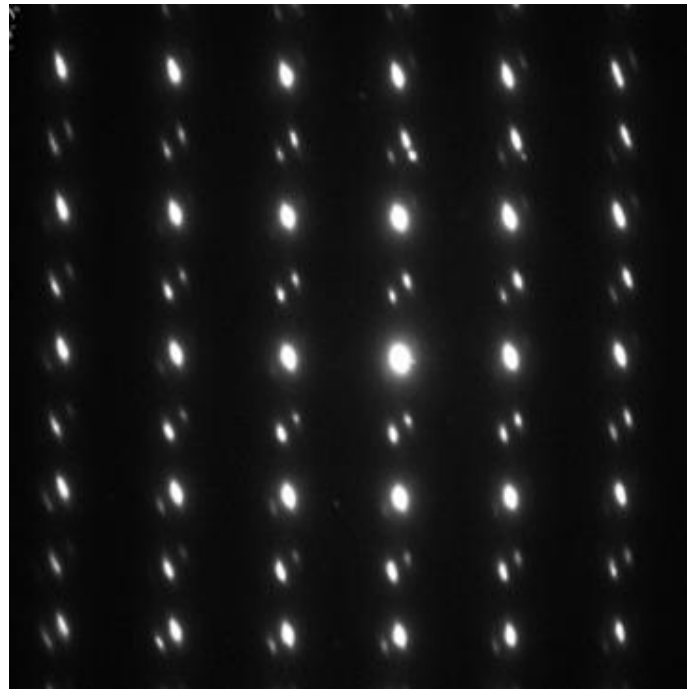


Figure 4.4.5 Electron diffraction pattern for Ag 54±1 at.% Pt, heat treated at 750°C for 60 days, possibly viewed along the $[100]_{\text{fcc}}$ zone axis.

The FIB SEM could be used to select the third phase for preparation of TEM specimens. Numerous zone axis electron diffraction patterns were obtained. For both compositions, each diffraction pattern showed doubling of spots or satellites or streaks, as seen also in the specimens prepared by PIPs. Two examples are shown in Figure 4.4.6.

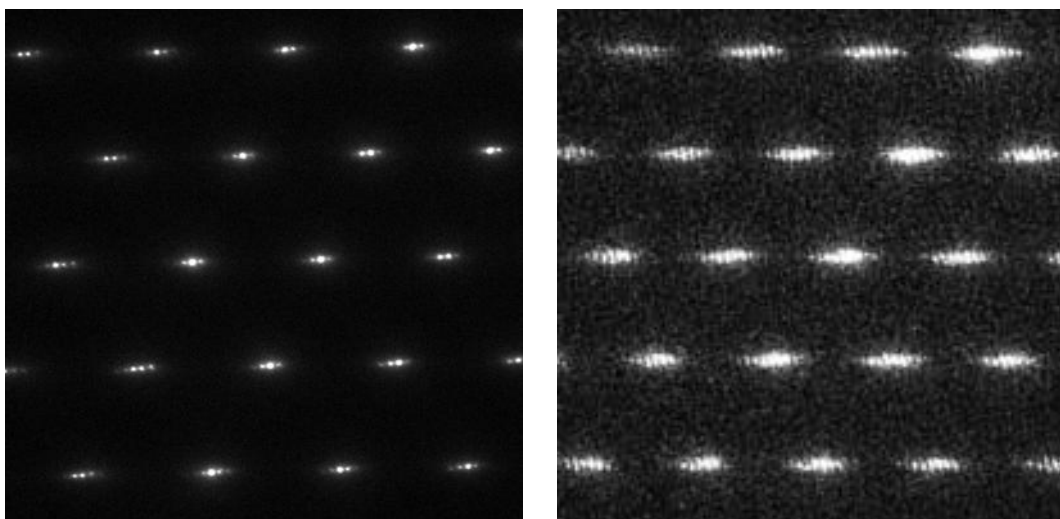


Figure 4.4.6 Electron diffraction patterns for (a) Ag 54 ± 1 at.% Pt after 60 days at 750°C , prepared by FIB SEM; (b) Ag 51 ± 1 at.% Pt after 80 days at 750°C , prepared by PIPS.

The possibilities of preparation artefacts and double diffraction were considered. Possible electron diffraction patterns, expected if an $L1_1$ structure is present, were modelled as shown in Figure 4.4.7 (a) below. Figure 4.4.7 (b) shows an experimental diffraction pattern from Ag 54 ± 1 at.% Pt after 60 days at 750°C , which appears closely similar. Considerable experimentation failed to demonstrate reproducibility: hundreds of experimental diffraction patterns did not repeat this similarity. This shows how difficult it was to obtain a suitable diffraction pattern.

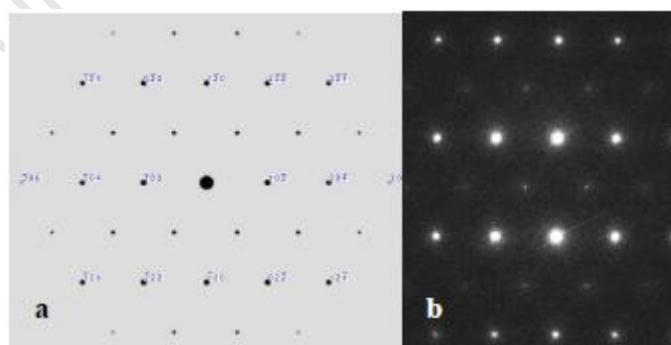


Figure 4.4.7 (a) Simulated electron diffraction pattern showing additional spots expected from $L1_1$ in $[112]$ zone axis diffraction pattern; (b) experimental diffraction pattern.

High magnification bright-field TEM images from the third phase revealed a fine-scale modulation, as shown in Figure 4.4.8 below.

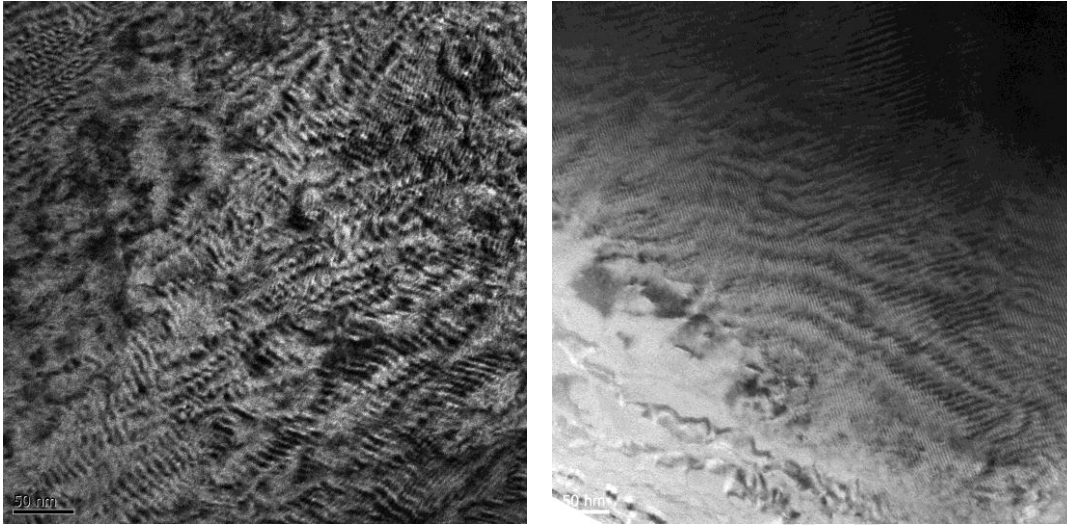


Figure 4.4.8 Bright-field TEM image of (a) Ag 51 ± 1 at.% Pt after 80 days at 750°C ; and (b) Ag 54 ± 1 at.% Pt after 60 days at 750°C , showing modulated microstructure.

5 DISCUSSION

5.1 EFFECT OF HEAT TREATMENT ON MICROSTRUCTURE

The as-cast specimens both showed a platinum-rich phase coexisting with a silver-rich phase, demonstrating the miscibility gap which exists near the 50:50 composition at moderate temperatures. The alloy with composition closest to 50:50, Ag 51±1 at.% Pt, also showed a third phase in the as-cast state which suggests that this phase formed on cooling from the melt. This third phase, of composition close to 50:50, developed and grew with heat treatment at 750°C for both alloys (appearing first after 40 days at this temperature, in the 54±1 at.% alloy). Some variation in the apparent volume fraction of the third phase was observed, but is probably within experimental variation in the sampling of sections of the alloys.

The composition of the third phase has been measured at Ag 52±1 at.% Pt for most of the alloys which is consistent with the 53 at.% noted by Durussel and Feschotte³.

Heat treatment at 850°C resulted in dissolution of the third phase for both alloys. It can therefore be concluded that the equilibrium state of both alloys, below 850°C, contains the third (near 50:50) phase. Consideration of the phase diagram leads to the conclusion that below 850°C only two phases should exist in the (platinum-rich) experimental alloys (the line compound and the platinum-based solid solution phase). The kinetics appear to be very slow and the three phases that were observed may take considerably more than 80 days to resolve to two phases.

5.2 HARDNESS

An increase in hardness after heat treatment may indicate the development of ordering in many systems²², as a result of a mixed state of order and disorder, or as a result of increased hardness of the ordered phase with increasing order, or both. The hardness of the experimental Ag-Pt alloys is seen to increase with length of heat treatment at 750°C. This is consistent with the observed increase in volume fraction of the third phase, observed by SEM and EDS.

The decrease in hardness observed after heat treatment at 850°C is observed after the same heat treatments which show dissolution of the third phase, with which the

increased hardness is concluded to be associated. The decrease in hardness could be also be due to recrystallisation.

5.3 DSC

The peaks of the DSC curves in both Figure 4.3.1 and 4.3.2 are seen to move to the right with increasing heat treatment time, indicating that the attainment of equilibrium, and dissolution of the third phase, is progressing and may not yet be complete after 80 days at 750°C. The peak heights observed are at 843°C and 851°C respectively, which is much higher than the transformation temperature on the phase diagram of 803°C. The third phase that was observed in the present work therefore appears to be the third phase in the phase diagram, a line compound with a dissolution temperature around 850°C.

5.4 TEM

Electron diffraction did not reveal the expected reflections associated with an ordered structure; nor were the observed diffraction patterns consistent with the simulated diffraction patterns of the L1₁ structure, except in one instance. The reason for the one occurrence could be that the alloy was homogenised before the long heat treatments. This was not repeated therefore the result was not reproduced. It was very difficult to find different zone axes with these extra reflections.

Another possible cause of the satellite peaks and additional doublets observed in many of the diffraction patterns is spinodal decomposition. This is typically observed as a compositional modulation with a very small wavelength²⁶. Although it was outside the scope of the current project to investigate this in detail, examination of Figure 4.4.4 (both bright field and dark field) reveals an apparent modulation of less than 10 nm. Higher magnification images in Figure 4.4.8 show these modulations more clearly. Comparison with the study by Hsiung and Zhou²⁶ shows remarkable similarities in both images and diffraction patterns, as shown in Figure 5.4.1. Hsiung and Zhou²⁶ concluded that spinodal decomposition was the reason for the modulation as well as the satellites as shown overleaf.

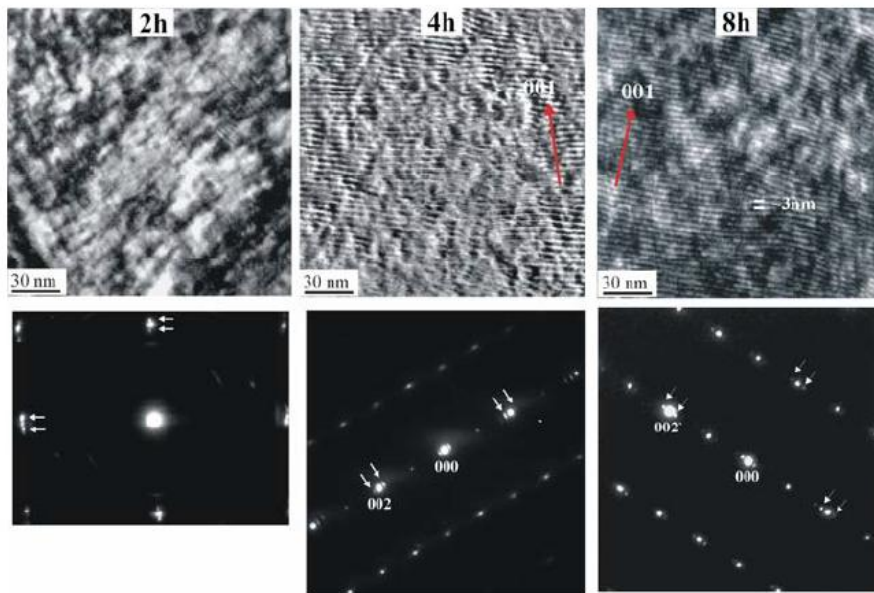


Figure 5.4.1 TEM bright-field images and electron diffraction patterns, acquired from a U-6wt%Nb alloy after ageing (after Hsiung and Zhou²⁶).

5.5 OVERVIEW

The work presented here has confirmed the presence of a third phase in Ag-Pt alloys near the 50:50 composition, at temperatures up to about 850°C. The kinetics of phase transformations in this system are very slow. The experimental results strongly indicate that the final, equilibrium state of the third phase was not attained within this project; furthermore, a complex process of spinodal decomposition and ordering appears to be underway. The final, thermodynamically stable state of the 50:50 alloy may be the predicted $L1_1$ superlattice, but this was not experimentally realised in the present work.

6 CONCLUSIONS

The objectives of this research were to:

- Confirm the presence of an ordered phase at or near the equiatomic composition in the Ag-Pt system
- Determine the structure of the ordered phase
- Evaluate the equiatomic region of the most recent phase diagram.

This research has led to the following preliminary conclusions:

- A third, ordered phase exists in the Ag-Pt system which appears to approach a single composition of Ag 52 ± 1 at.% Pt, with extended heat treatment.
- Electron diffraction patterns showed split and satellite additional reflections, which could not definitively be identified with an orthorhombic structure such as the $L1_1$ ordered structure except for one diffraction pattern.
- The electron diffraction patterns, and TEM images, suggest that spinodal decomposition may be occurring.
- The equiatomic composition region of the phase diagram may need revision, but further work will be required to identify the composition of the third phase unambiguously.

This work therefore confirms the existence of a line compound near the 50:50 composition, but is not able to conclusively associate this line compound with either the structure reported by Durussel and Feschotte³, or the $L1_1$ structure predicted by Nelson *et al.*¹. Spinodal decomposition should be investigated as a possible cause of the observed electron diffraction effects, as detailed in the next section.

7 RECOMMENDATIONS

The conclusions of the present work should be extended to a full understanding of the third phase: its kinetics of formation, mechanism of formation, and final structure. The figures which follow are electron patterns from this work, together with the work of Professor Jan Neethling of Nelson Mandela Metropolitan University: modelled electron diffraction patterns and atomic models, created in order to understand the experimental results. The intention of this presentation is to allow further work to be done, using all efforts to date as a basis.

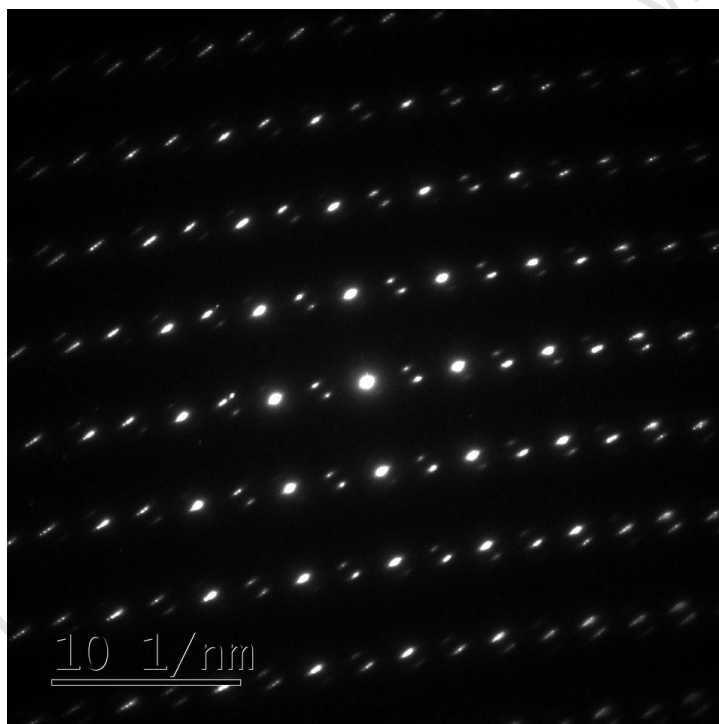


Figure 7.1 SAD of AgPt phase; the satellite spots are most likely generated by spinodal decomposition; however more diffraction studies are required.

The electron diffraction investigation of the AgPt phase was complicated by the fact that no sharp Kikuchi lines were visible in the diffraction patterns and therefore no diffraction patterns could be recorded with the electron beam parallel to a zone axis. The diffraction patterns also exhibit extra satellite spots which made the identification of a single phase impossible²⁸.

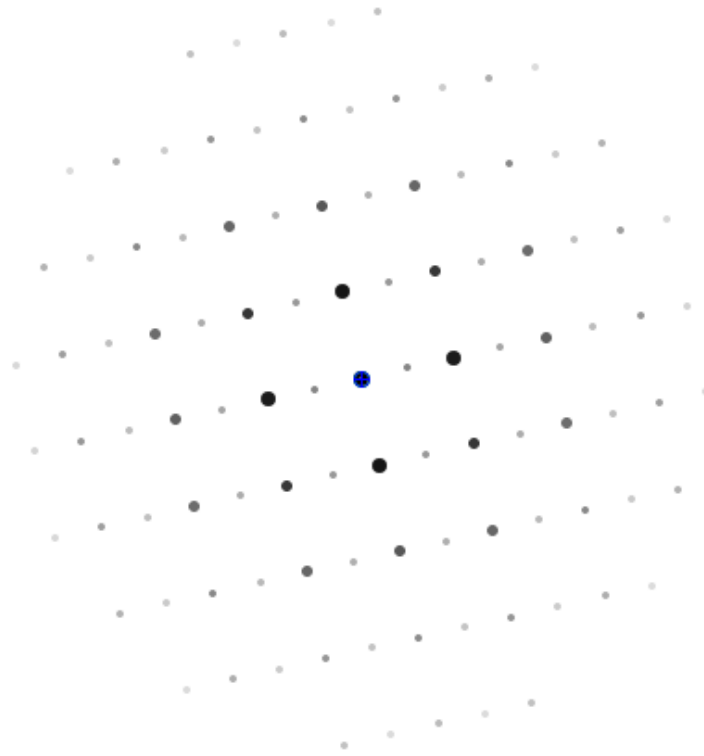


Figure 7.2 Simulated [100] zone axis diffraction pattern of AgPt, calculated by using a FePt $L1_0$ unit cell, which was modified for AgPt with lattice parameters adjusted to $a = 0.42$ nm and $c = 0.40$ nm²⁷.

It was not possible to index the SADs using the normal FCC structure of AgPt or the $L1_1$ AgPt unit cell structure. The best match of the strong reflections in the SADs was obtained with an FCC structure of Ag or Pt with slightly larger lattice parameter of $a = 0.42$ nm. Since the SADs exhibit closely spaced satellite spots, splitting of spots and possible superlattice spots, which indicates some atomic ordering in the $\langle 010 \rangle$ direction, it was decided to use an $L1_0$ unit cell for AgPt with $a = 0.42$ and $c = 0.40$ nm. In the $L1_0$ structure, monoatomic planes are stacked along the $[001]$ direction. In addition to the $L1_0$ structure, the SAD patterns recorded along (not exactly) the $[100]$ and $[101]$ directions (see Fig. 7.1 and Fig. 7.3) exhibit satellite spots which could be due to composition modulation due to spinodal decomposition²⁸.

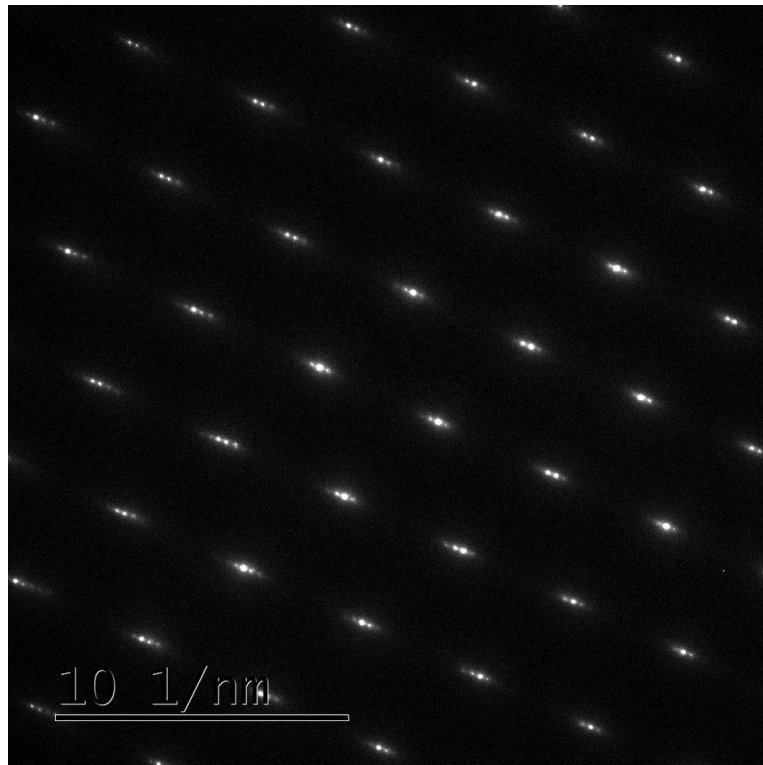


Figure 7.3 SAD pattern of AgPt showing closely spaced satellite spots on either side of the main spots. The satellite spots are most likely due to a composition modulation such as spinodal decomposition.

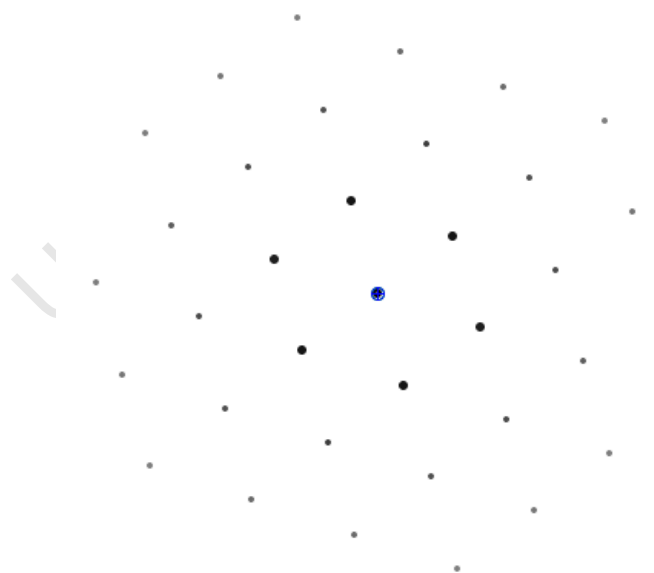


Figure 7.4 Simulated [101] zone axis diffraction pattern of AgPt, calculated by using a FePt $L1_0$ unit cell, which was modified for AgPt with lattice parameters adjusted to $a = 0.42$ nm and $c = 0.40$ nm²⁷. This zone axis is the best match for Fig. 7.3.

The following structures were simulated for the $L1_1$ structure as well as the $L1_0$ structure for the AgPt system with adjusted lattice parameters of $a = 0.42$ nm and $c = 0.40$ nm.

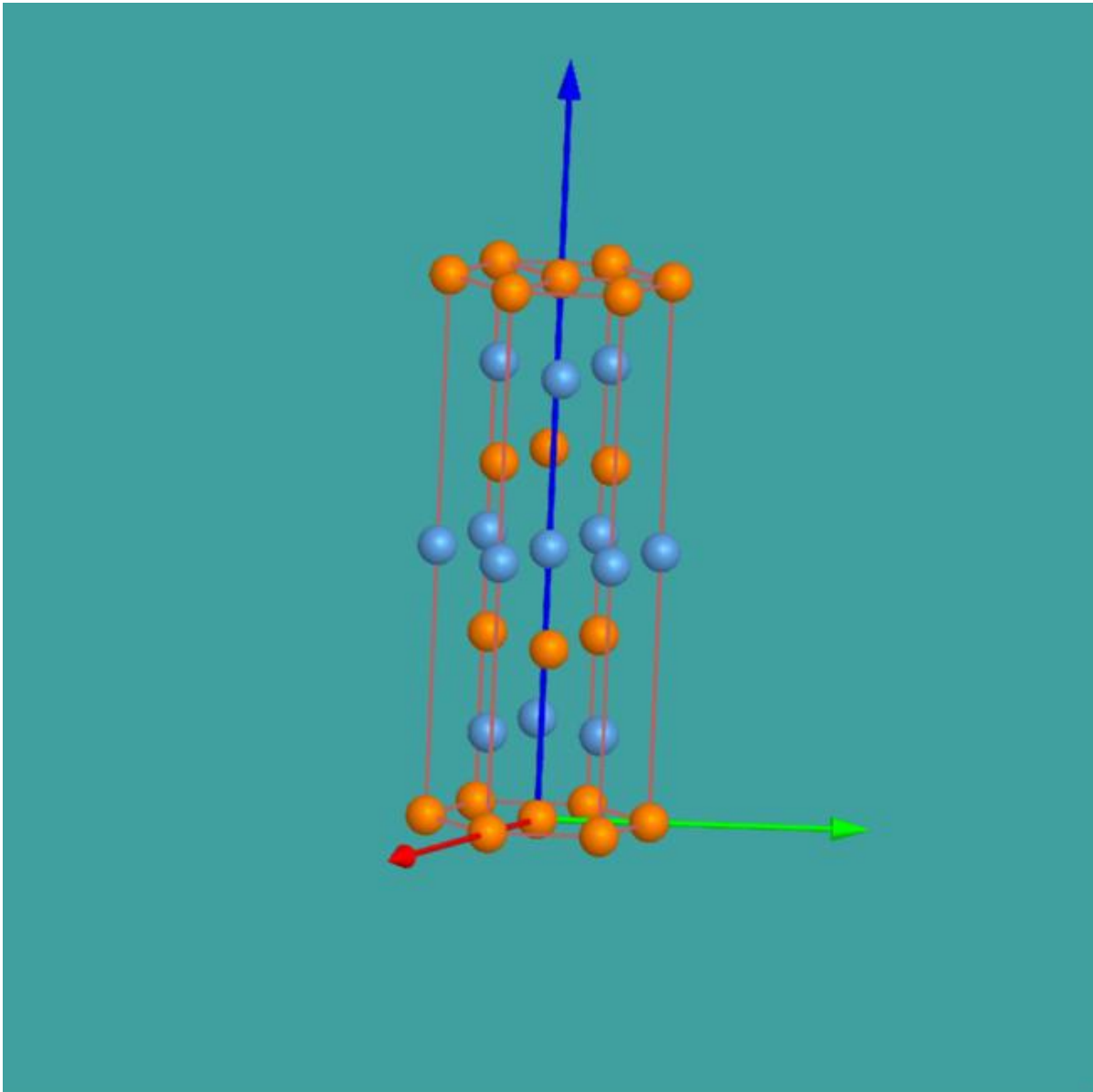


Figure 7.5 Simulated structure for AgPt $L1_1$ based on CuPt $L1_1$ structure²⁷.

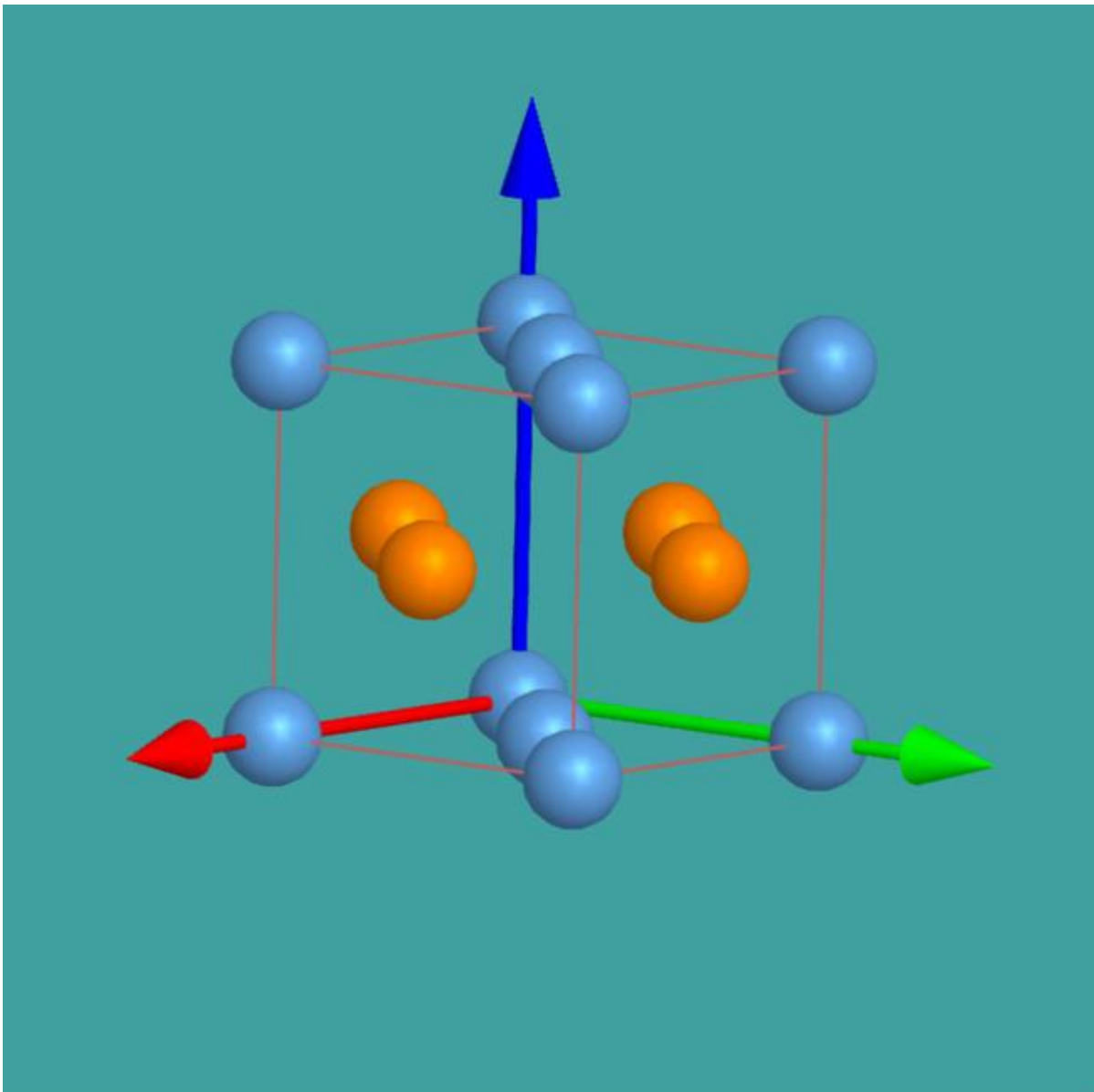


Figure 7.6 Simulated unit cell for AgPt L1₀ structure; adapted from FePt L1₀²⁷.

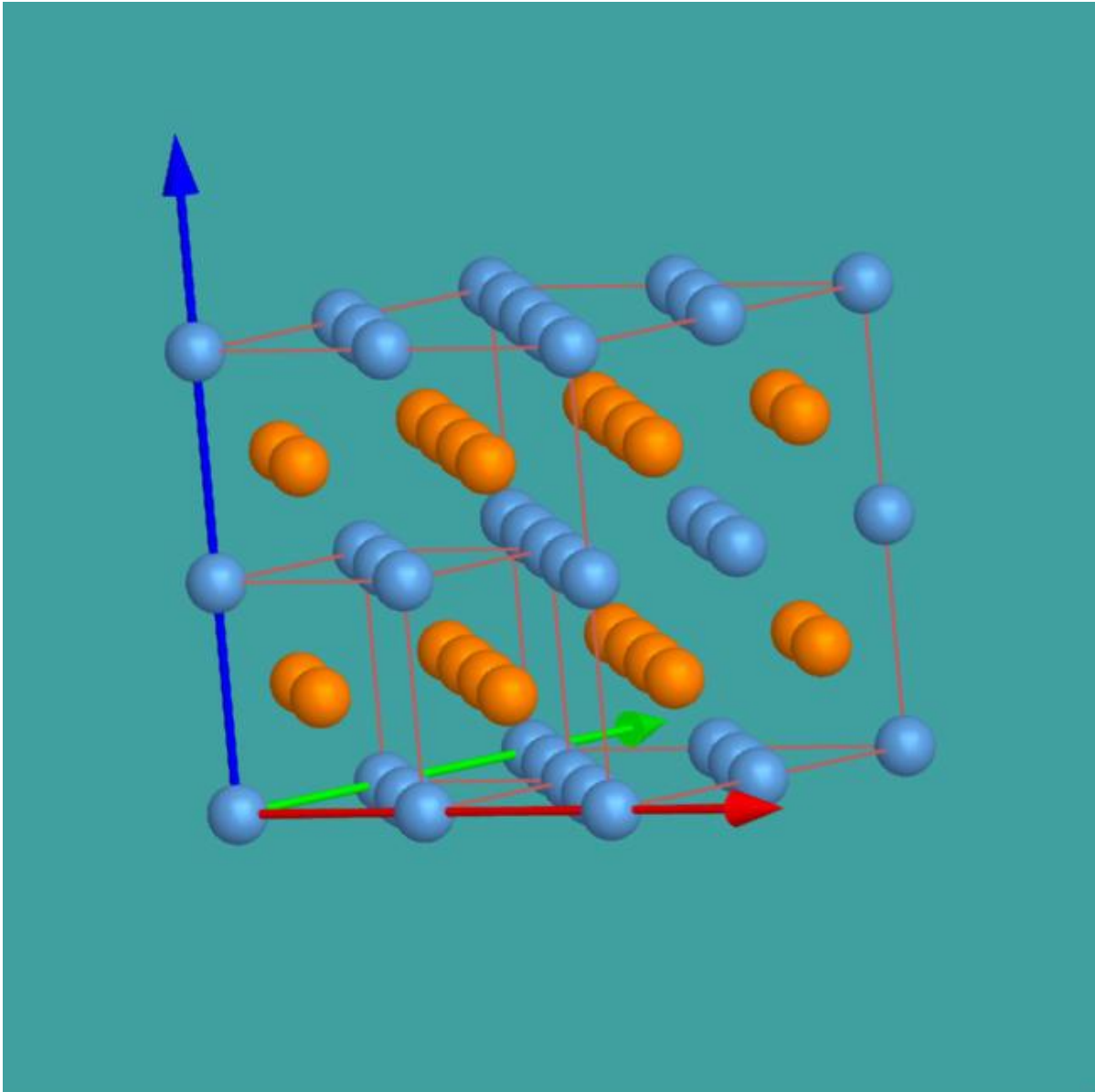


Figure 7.7 Simulated AgPt L₁₀ structure adapted from FePt L₁₀²⁷.

8 REFERENCES

1. L. J. Nelson, G. L. W. Hart and S. Curtarolo, *Physical Review B*, 2012, **85**, 9.
2. J. Matthiessen, *Chem. Soc.*, 1867, **20**, 201-220.
3. P. Durussel and P. Feschotte, *Journal of Alloys and Compounds*, 1996, **239**, 226-230.
4. J. H. Thompson and E. H. Miller, *J. Am. Chem. Soc.*, 1906, **28**, 1115.
5. F. Doerinckel, *Z. Anorg. Chem.*, 1907, **54**, S. 341.
6. N. S. Kurnakow and W. A. Nemilow, *Z. Anorg. Chem.*, 1928, **168**, 339-348.
7. C. H. Johansson and J. O. Linde, *Ann. Phys.*, 1930, **6**, 458-488.
8. J. Banhart, W. Pfeiler and J. Voitländer, *Physical Review B*, 1988, **37**, 6027-6029.
9. A. Schneider and U. Esch, *Z. Elektrochem.*, 1943, **49**, 73-89.
10. O. A. Novikova and A. A. Rudnitskii, *J. Inorg. Chem. USSR*, 1957, **2**, 208-221.
11. W. Klement and H. L. Luo, *Trans. Met. Soc. AIME*, 1963, **227**, 1253-1254.
12. M. Hansen and K. Anderko, *Constitution of Binary Alloys*, McGraw-Hill, New York or General Electric Co., Business Growth Services, Schenectady, New York, 1958.
13. H. Ebert, J. Abart and J. Voitlander, *Journal of the Less-Common Metals*, 1983, **91**, 89-96.
14. R. Erni, T. Etter, H. Heinrich and G. Kostorz, *Zeitschrift Fur Metallkunde*, 2001, **92**, 1194-1196.
15. I. Karakaya and W. Thompson, *Journal of Phase Equilibria*, 1987, **8**, 334-340.
16. S. Takizawa, K. Terakura and T. Mohri, *Physical Review B*, 1989, **39**, 5792-5797.
17. C. S. Barrett and T. B. Massalski, *Structure of metals: Crystallographic Methods, Principles and Data*, Pergamont Press, Oxford, 1980.
18. M. H. F. Sluiter, C. Colinet and A. Pasturel, *Physical Review B*, 2006, **73**, 17.
19. X. S. Yan, P. Lin, X. Qi and L. Yang, *International Journal of Materials Research*, 2011, **102**, 381-388.
20. M. W. Finnis and J. E. Sinclair, *Philosophical Magazine A-Physics of Condensed Matter Structure Defects and Mechanical Properties*, 1984, **55**, 45-55.
21. G. L. W. Hart, *Nat Mater*, 2007, **6**, 941-945.
22. P. R. Subramanian, *J. Phase Equilib.*, 1993, **14**, 62-75.
23. A. Schneider and U. Esch, *Z. Elektrochem.*, 1944, **50**, 290.
24. H. Lang, T. Mohri and W. Pfeiler, *Intermetallics*, 1999, **7**, 1373-1381.

References

25. J. M. a. P. M. G. Klančnik, *RMZ – Materials and Geoenvironment*, 2010, **57**, 127-142.
26. L. Hsiung and J. Zhou, University of California, Editon edn., 2006.